JAERI-M
82-115

ANALYSIS OF PKL TEST K9 BY THYDE-P CODE
(CSNI ISP NO.10 AND THYDE-P SAMPLE CALCULATION RUN 70)

September 1982

Seiji KOSUGI, Shinobu SASAKI and Yoshiro ASAHI

日本原子力研究所
Japan Atomic Energy Research Institute

JAERI-Mレポートは，日本原子力研究所が不定期に公刊している研究報告書です。
入手の問合わせは，日本原子力研究所技術情報部情報資料課（〒319-11茨城県那珂郡東海村）あて，お申しこしください。なお，このほかに財団法人原子力弘済会資料センター（〒319-11 茨城県那珂郡東海村日本原子力研究所内）で複写による実費頒布をおこなっております。

JAERI-M reports are issued irregularly.
Inquiries about availability of the reports should be addressed to Information Section, Division of Technical Information, Japan Atomic Energy Research Institute, Tokai-mura, Naka-gun, Ibaraki-ken 319-11, Japan.

編集兼発行　日本原子力研究所
印　　刷　㈱高野高速印刷

JAERI-M 82-115

Analysis of PKL Test K9 by THYDE-P Code
(CSNI ISP NO.10 and THYDE-P Sample Calculation Run 70)

Seiji KOSUGI, Shinobu SASAKI and Yoshiro ASAHI

Division of Nuclear Safety Evaluation,
Tokai Research Establishment, JAERI

(Received August 5, 1982)

An analysis of PKL Test K9 is made by the THYDE-P code. Test K9 is the Standard Problem No.10 of Committee on the Safety of Nuclear Installations (CSNI) in the Nuclear Energy Agency (NEA), OECD. The objective of Test K9 is to investigate gravity-feed refill and reflood processes following a double-ended guillotine break in a cold leg with emergency cooling water being injected into the intact cold legs. THYDE-P is a code to analyze both the blow-down and refill-reflood phases of loss-of-coolant accidents (LOCAs) of pressurized water reactors (PWRs). In this report, calculated results are compared with the experimental data and discussed for the purpose of verification study and model development of THYDE-P. A good agreement with the experimental data was obtained using the best estimate (BE) options.

Keywords: LOCA, PKL, THYDE-P Code, PWR, Refill, Reflood, Verification Study, ISP NO.10, Reactor Safety

THYDE－PコードによるPKLテストK９の解析
（CSNI国際標準問題№10及びTHYDE－Pサンプル計算70）

日本原子力研究所東海研究所安全解析部
小杉　誠司・佐々木　忍・朝日　義郎

（1982年8月5日受理）

ＰＫＬテストＫ９の解析をTHYDE－Pコードを用いておこなった。テストＫ９は，OECD－NEA－CSNIの国際標準問題№10である。実験の目的は，重力注水による再浸水・再冠水過程を研究することにあり，両端ギロチン破断がコールドレグに起ったとして，緊急炉心冷却水をコールドレグに注入している。THYDE－Pは，加圧水型軽水炉の冷却材喪失事故におけるブローダウン及び再浸水・再冠水過程を解析するコードである。

本報告では，THYDE－Pの検証及びモデル開発のために，計算結果と実験値を比較し，検討した。最適評価オプションを用いることによって，実験値との良い一致が得られた。

CONTENTS

目　　次

LIST OF TABLES

LIST OF FIGURES

1. Introduction

An analysis of PKL (Primärkreisläufe = primary loops) experiment K9 has been performed with the THYDE-P code[1]~[6] to verify the system performance of THYDE-P and also to obtain better understanding of the experiment.

The PKL facility is to simulate the thermohydraulic behavior during a LOCA with ECC water injection for typical West German 1300 MW PWRs. The objective of Test K9 was to investigate the gravity-feed refill and reflood processes, which was adopted as the OECD-NEA-CSNI ECCS Standard Problem No.10[7]~[10].

THYDE-P has been applied to various experiment analyses for its verification and model refinement. For example Loss-of-Fluid Test (LOFT) experiments have been analyzed using THYDE-P by Hirano et al.[3],[4],[6]. However, the refill and reflood processes with a long period of time could not be in depth investigated in the above analyses. Thus the present K9 analysis is one of the important mile stones in the course of THYDE-P development.

Test K9 was carried out with an initial condition corresponding to the system status at the end of blowdown and just prior to the refill and reflood phase during a postulated double ended cold leg break. On the other hand, THYDE-P is not designed to start its calculation with such an initial condition as above. Rather, THYDE-P has been developed to have a capability a through analysis from blowdown to refill and reflood phases. Therfore, a fictitious blowdown from a system pressure of 160 bar was assumed in the present analysistto have occurred in the PKL facility which was then analysed by THYDE-P. The conditions of this ficitious blowdown were so adjusted that the analytical results at the end of blowdown came as close as possible to the PKL experimental initial condition. In this adjustment, particular attention was given to the flow rate at the break, system pressure and the heater rod temperature. After such preliminary procedures, the calculation was futher performed to obtain the relevant results to the K9 experiment which were then compared with the experimental results.

The thermal-hydraulic calculation in THYDE-P has in principle been based on a homogeneous equilibrium model. However, a time delay model for the density change has been incorporated in order to avoid the large pressure drop due to very radid vapor condensation near the ECCS injection point. Since there is only limitted theoretical basis to determine

the delay parameter so far, in the present calculation, the values of the delay parameters were empirically determined. A physical model to estimate the delay parameter is now under development. Futhermore several models newly implemented (phase separation model at the downcomer top and minimum film boiling temperature) are still rather crude and futher investigations and developments are now in progress. Therefore, the present analysis should be regarded as an interim one.

The outline of this report is as follows: In chapter 2 a brief description of the Standard Problem No.10 is presented while the models used in the present analysis and the preparation of the input data are given in chapters 3 and 4, respectively. In chapter 5, the calculated results are compared with the experimental data. Finally, in chapter 6, we present our conclusions.

2. Brief Description of PKL Test K9

2.1 Primary Objectives and Features

The objective of the integral cold leg injection Test K9 (200% double ended break) was to investigate the gravity-feed refill and reflood processes at the later portion of a LOCA in a PWR, and to provide data primarily to verify computer codes describing the refill and reflood phases in the course of the accident.

Test K9 differs from other cold leg injection tests in the same facility in the following aspects:

(1) A uniform radial power profile in the core.
(2) An increased temperature of injected Emergency Core Cooling (ECC) water from 35 to 53°C.
(3) An injection mass flow rate was reduced to one third of which history corresponds to that of a typical US-PWR.
(4) Somewhat higher maximum initial clad temperatures in the bundle (about 600°C)
(5) A smaller bundle heating power during the initial phase (1327 KW).

2.2 Test Facility

PKL-facility simulates the essential primary system components of a typical West German 1300 MW PWR with regard to their thermohydraulic behaviour. The facility consists of the pressure vessel with the heater bundle, the downcomer simulator, the primary loops with components of the steam generator and pump simulator, the injection devices, the break geometry simulator, the separators, and the test containment to maintain a back-pressure at the location of break (see Fig. 2.1). The number of heater rods and the horizontal cross sections of the test facility are scaled to 1:134 of a typical German PWR. The vertical geometries are full scale (see Fig. 2.2).

Inside the pressure vessel, the cylindrical core barrel is provided which encloses the octagonal inner casing (see Fig. 2.3). The space between the pressure vessel and the core barrel is sealed from the core region inside the inner core casing and from the upper and lower plenum. However, a pressure equalization line at the upper end of the pressure vessel is provided for pressure balance between the upper plenum and this annular gap. The rod bundle surrounded by the inner core casing

consists of 340 rods, 337 of which are electrically heated.

The downcomer was simulated by the downcomer nozzle region and the downcomer U-tube (see Fig. 2.2). The cold leg injection took place both directly in the downcomer nozzle region and the lines of the intact single and double loops near to the downcomer nozzle region. A cylindrical insertion and repulsing metal sheets are installed in the downcomer nozzle region in order to avoid the emergency cooling water directly flowing from the intact loop injection points into the broken loop (see Fig. 2.4).

The testing plant consists of 3 loops: the brocken loop, the intact single loop and the intact double loop which bas double capacity in order to simulate 2 primary loops of a PWR. Cross-sections and lengths of the primary loop lines have been designed so as to result in flow losses being approximately equal to those arising in the corresponding lines of the reactor plant. For simulating the double ended break, the break location is in a cold leg between the pump simulator and the downcomer nozzle region. The steam generator U-tube are inserted in the heat exchangers and the number of U-tubes is scaled to 1:134 of the reactor steam generator. The secondary side of the steam generators is filled to above the tubes with water and over that with saturated steam.

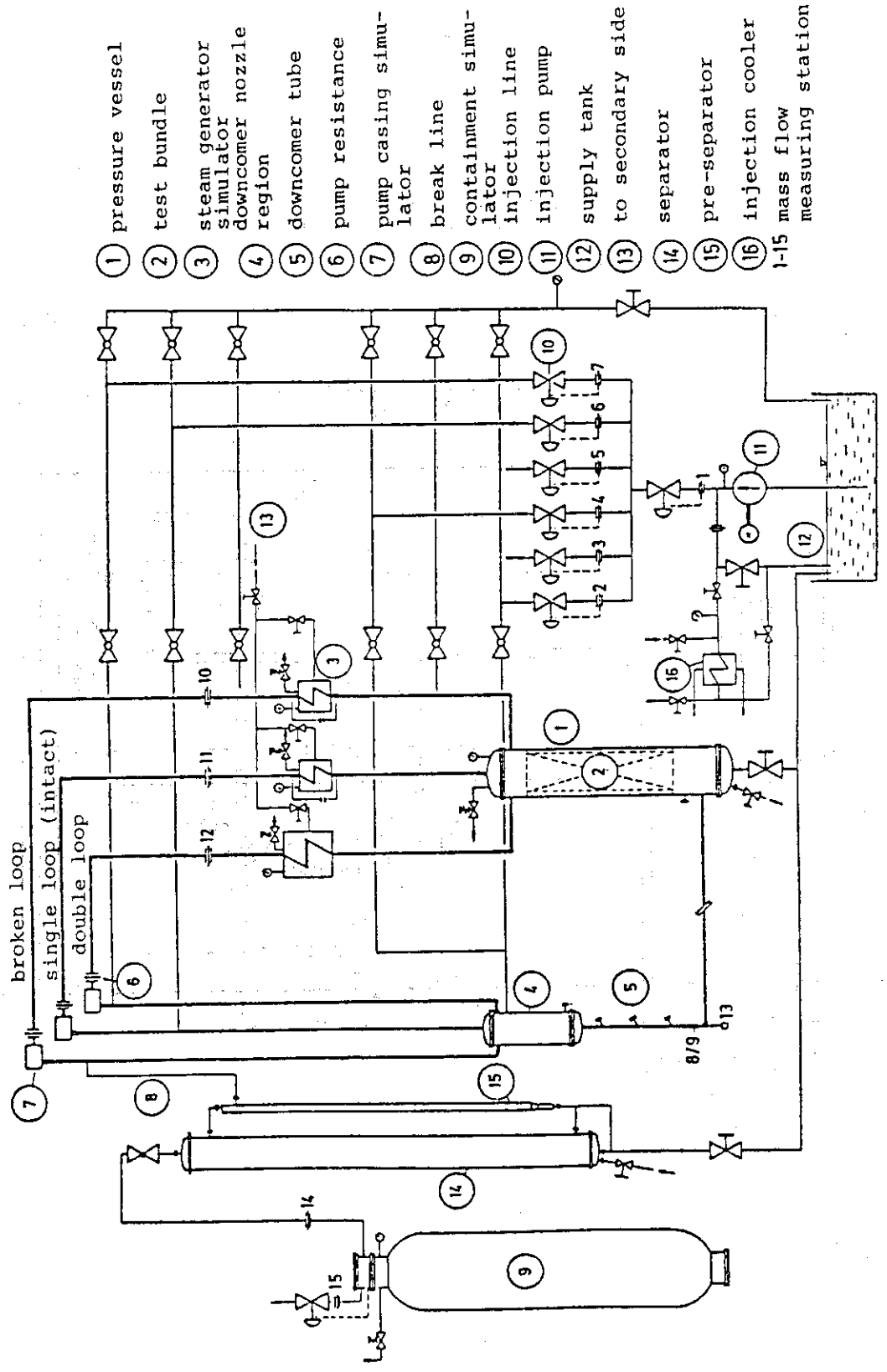

Fig. 2.1 PKL-Schematic with Mass Flow Instrumentation

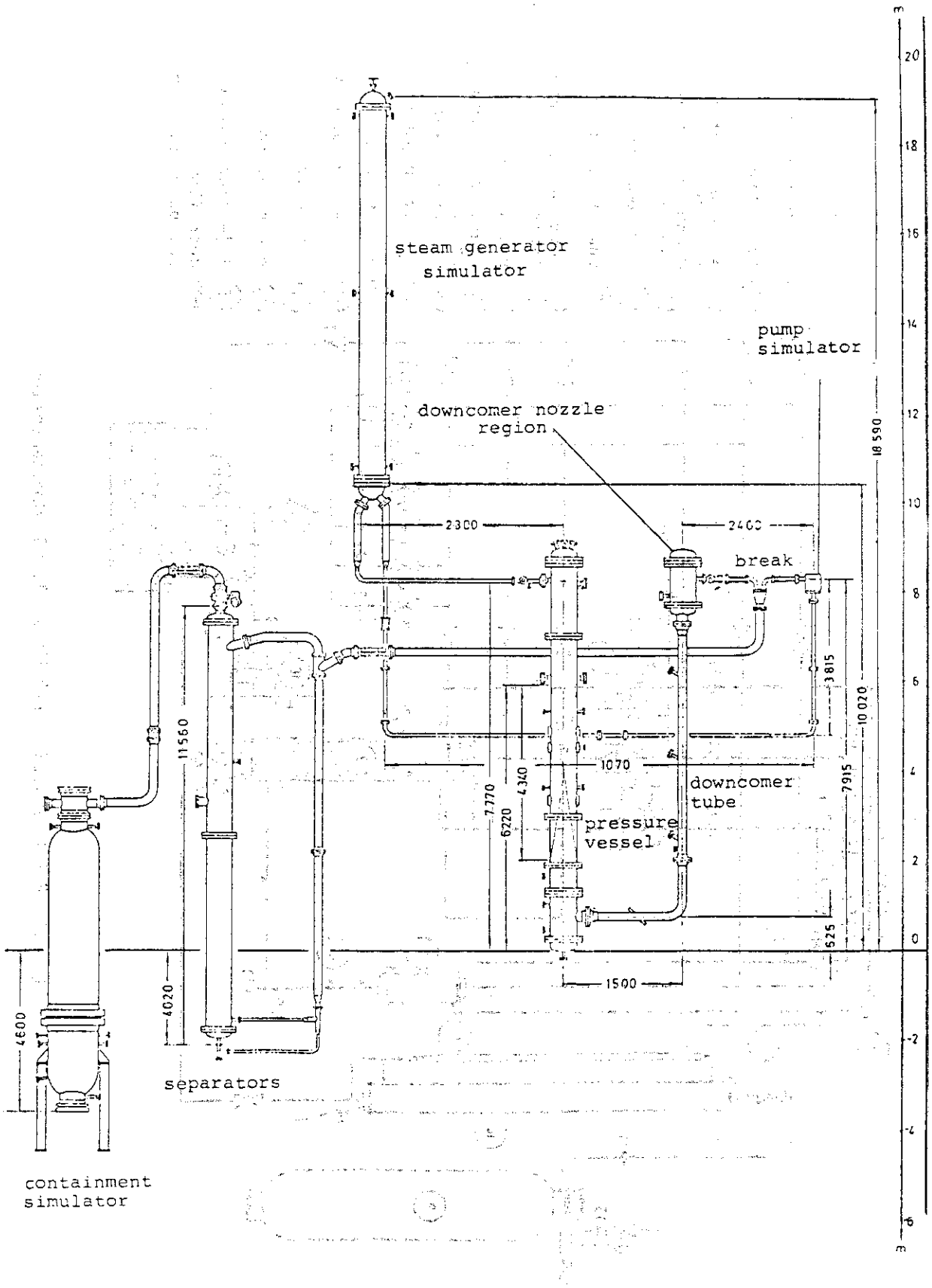

Fig. 2.2 Elevations of PKL-Components

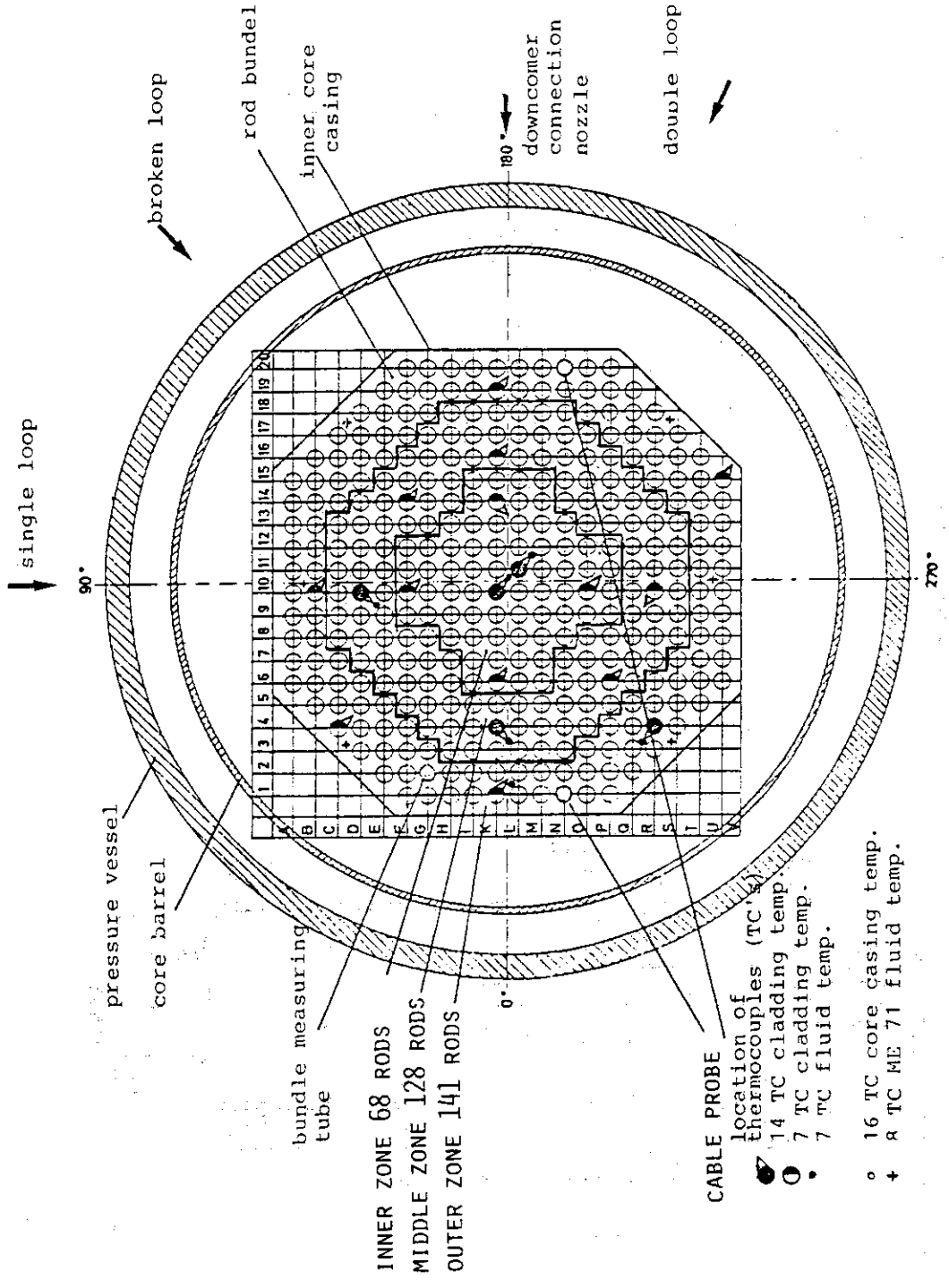

Fig. 2.3 Cross Section of Pressure Vessel

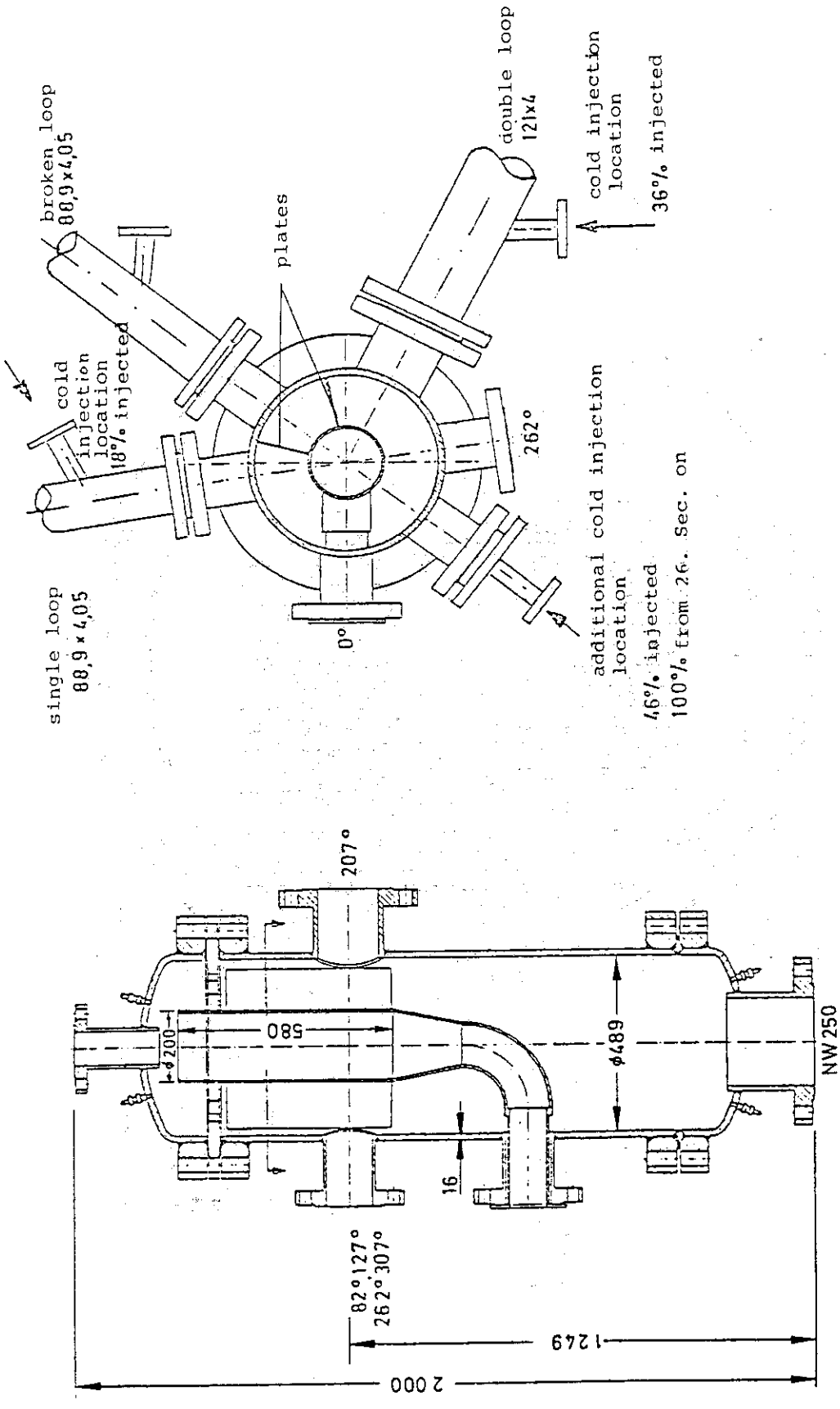

Fig. 2.4 Downcomer Nozzle Region with Cold Leg Injection Locations

2.3 Initial and Boundary Conditions

As has been mentioned in chapter 1, there are three kinds of "initial conditions" in the present analysis as follows:

(1) the initial conditions of the experiment.

(2) the initial conditions of the calculation which corresponds to those of the experiment.

(3) the initial conditions of the fictious blowndown in the calculation which is assumed in order to obtain the initial conditions (2) mentioned above.

Initial and boundary conditions of Test K9 are shown in Table 2.1. The brief comparison of the initial conditions between Test K9 and the calculation, (2) above, are shown in Table 2.3. The initial conditions of the fictious blowdown in the calculation are shown in Appendix A, together with other input data.

Table 2.1 Initial and Boundary Conditions of Test K9

Test Parameters	Experiment
Location of break	cold leg between pump and reactor pressure vessel
Break size	double ended guillotine
Initial pressure at break location	4.5 bar
Pressure history at the break ("containment pressure")	see Fig. 2.5
Total bundle power at initiation of test	1.327 MW
History of heating power	see Table 2.2
Power supply (initial value)	
— inner zone	3.98 KW/rod
— middle zone	3.93 KW/rod
— outher zone	3.92 KW/rod
Initial heater rod temperature on the average	
— in the final stage	410 ± 3°C
— in the middle stage	600 ± 5°C
— in the initial stage	340 ± 3°C
Cold leg injection	
— broken loop	no
— intact single loop	yes
— intact double loop	yes
— downcomer nozzle region	yes

Hot leg injection	no
Temperature of injection water	varies between 50.50°C and 53.6°C and is on the average equal to (53 ± 3)°C
Injection mass flow rates	shown in Fig. 2.6 (decreasing from 22 kg/sec at the beginning and constant = 1.9 kg/sec from appr. 30 sec on)
Steam generator secondary side	
broken loop — initial temperature	267.5°C
— initial pressure	53 bar
— water level	7.5 m
intact single loop	
— initial temperature	270.5°C
— initial pressure	55.5 bar
— water level	7.8 m
intact double loop	
— initial temperature	270.5°C
— initial pressure	55.5 bar
— water level	7.6 m

Table 2.2 History of Heating Power per Rod

time (sec)	power (KW)
0	0
1.8	4.0
63.0	4.0
75.0	3.91
100.0	3.75
125.0	3.62
150.0	3.51
200.0	3.34
250.0	3.18
300.0	3.05
350.0	2.87

Table 2.3 Brief Comparison of the Initial Conditions between Test K9 and the Calculation

Parameter	Experiment	Calculation
Initial heater rod temperature (°C)		
— ME1	≈ 320	≈ 450
— ME2	≈ 430	≈ 520
— ME3	≈ 520	≈ 570
— ME4	≈ 600	≈ 610
— ME5	≈ 540	≈ 550
— ME6	≈ 480	≈ 490
— ME7	≈ 400	≈ 380
S.G. outlet temperature (°C)		
— intact loop	≈ 240	≈ 260
— broken loop	≈ 220	≈ 260
S.G. outlet mass flux ($kg/m^2 \cdot sec$)		
— intact loop	≈ 2	≈-0.1
— broken loop	≈ 2	≈ 2
Initial pressure at the break location (bar)	4.53	4.53
Initial pressure at the upper plenum (bar)	4.50	4.54

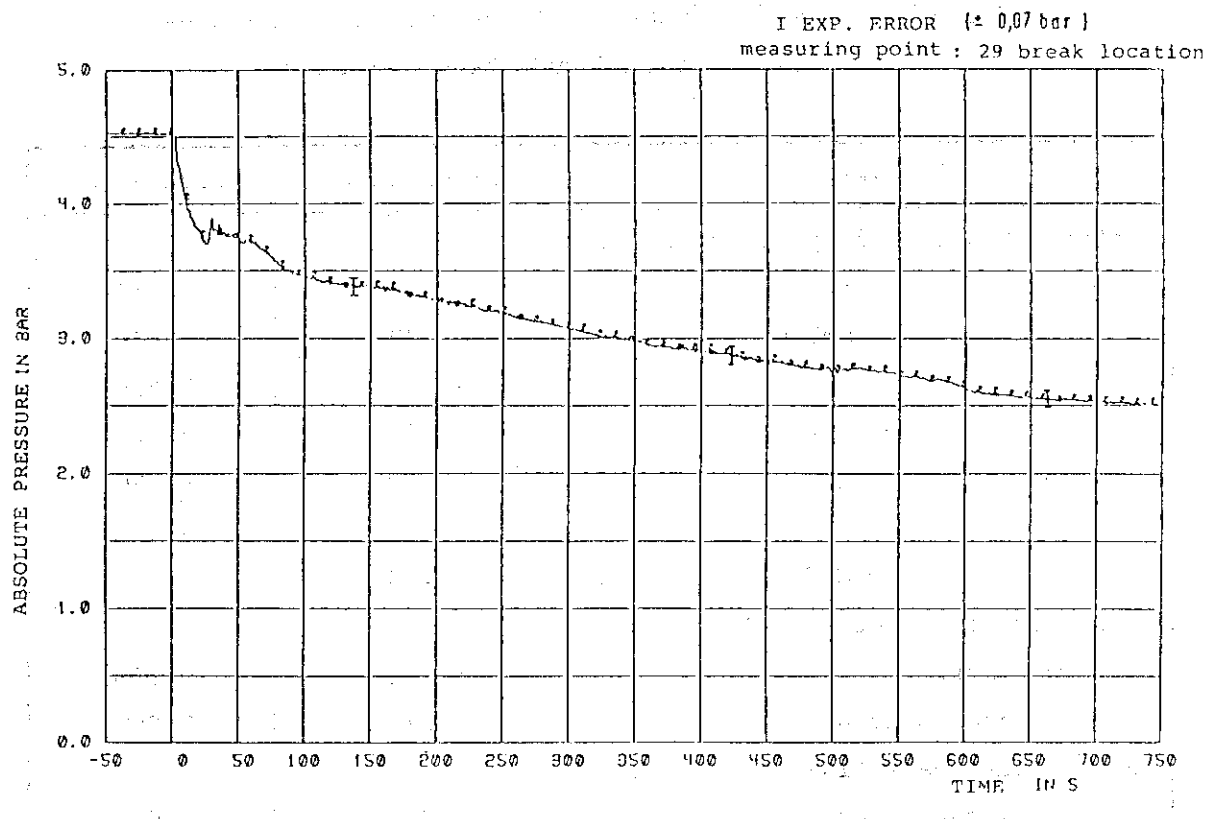

Fig. 2.5 Pressure History at Break Location

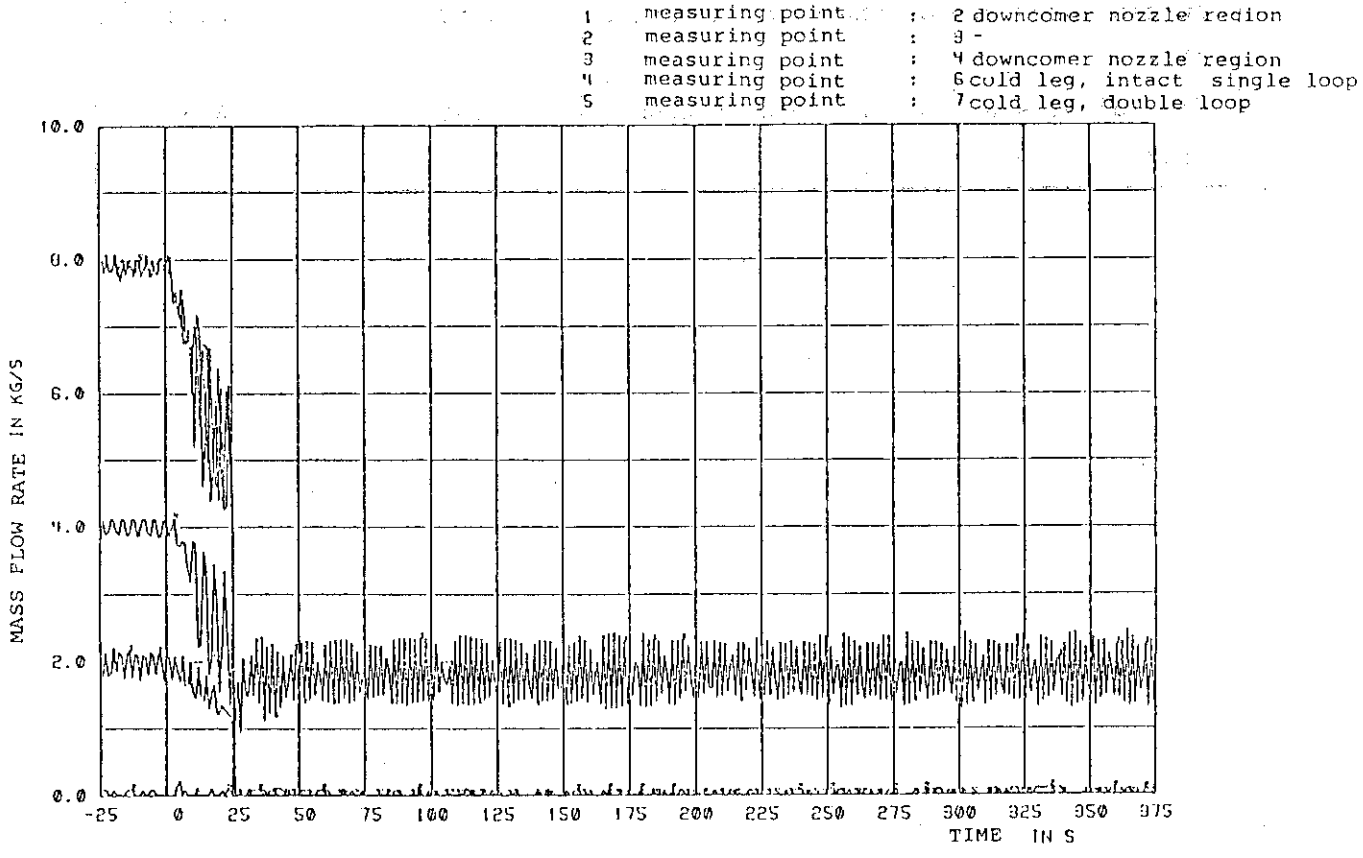

Fig. 2.6 Injection Rates of ECC Water

3. Models in Present Calculation

The models and methods of the THYDE-P code have been presented in detail in refs (1) to (6). In this section, several models newly developed for the present analysis are mainly described. These models will be incorpolated in a future version of THYDE-P.

3.1 Heat Transfer Correlations

The heat transfer correlations used in the present calculation are summarized in Tables 3.1 and 3.2. As has been already pointed out[3),(5)], the heat transfer mode 4-4 (pool transition boiling) plays an important role in the reflood calculation. In this mode, it is assumed that the Bromley-Pomerantz's correlation[15] is not applicable when coolant quality x is less than x_c. For simplicity in the present calculation, the heat flux is set to be a constant ϕ_c as follows[3]:

$$\phi = \phi_c \quad \text{when} \quad x < x_c \quad , \tag{3.1.1}$$

where

$$x_c = 0.1 \quad ,$$

$$\phi_c = 50 \text{ kcal/m}^2\cdot\text{sec.} \quad (64{,}000 \text{ Btu/ft}^2 \text{ sec.}). \tag{3.1.2}$$

Futhermore the idea of the minimum stable film boiling temperature is newly implemented (mode 4-5):

$$\phi = \phi_c \quad \text{when} \quad T_w < T_{MSFB} \quad ,$$

where T_{MSFB} is the minimum stable film boiling temperature which will be discussed in detail in subsection 3.5.

Table 3.1 Heat Transfer Correlations

Mode	Conditions		Correlations
	Coolant Condition	Other Conditions	
1	subcooled	$T_w < T_{sat}$	Dittus-Boelter[11]
2	subcooled	$T_w > T_{sat}$	Interpolation between Model and Mode3
3	saturated	$\phi < \phi_{CHF}$	Jens-Lottes[12]
4	saturated	$\phi > \phi_{CHF}$	(see Table 3.4)
5	superheated	Re < 3000	McEligot[13]
6	superheated	3000 < Re < 5000	McEligot[13]
7	superheated	Re > 5000	McEligot[13]

Table 3.2 Heat Transfer Correlations in Mode 4

Mode	Conditions	Correlations
4-1	$G > G_{min}$, $x > x_c$	Groenevelt
4-2	$G > G_{min}$, $x < x_c$	Forced convection transition boiling
4-3	$G < G_{min}$, $x > x_c$	Bromley-Pomeranz[15]
4-4	$G < G_{min}$, $x < x$	Pool transition boiling
4-5	$T_w < T_{MSFB}$	Pool transition boiling

T_w; Wall temperature

G_{min}; Minimum mass flux (300.0 kg/m^2·sec)

x_c; Threshold quality (=0.1)

3.2 Drift Flux Model

Since a drift flux model is used in THYDE-P, the terms due to drift velocity appear in energy and momentum equations. When the flow becomes stagnant, namely $G \approx 0$, the drift enthalpy flux I defined by

$$I = x\rho_{fs} u_{gj} (h_{gs} - h_{fs}) \quad , \tag{3.2.1}$$

where,

x ; quality

ρ_{fs}; density of saturated fluid

h_{gs}; specific enthalpy of saturated steam,

plays an important role.

Here the drift velocity u_{gj} is assumed to be given by

$$u_{gj} = u^0_{gj} S^2_\alpha = 1.41 \left[\frac{g\sigma(\rho_{fs} - \rho_{gs})}{\rho^2_{fs}} \right]^{\frac{1}{4}} S^2_\alpha \quad , \tag{3.2.2}$$

$$S_\alpha = 1 - \exp\{1 - (\frac{1-\alpha}{1-\alpha_c})\} \quad , \tag{3.2.3}$$

where,

ρ_{gs}; density of saturated steam

σ ; surface tension

g ; gravitational acceleration

α ; void fraction

The factor S_α is introudced so as to avoid the relative velocity defined by

$$u_{rel} = \frac{u_{gj}}{1-\alpha} \quad , \tag{3.2.4}$$

to diverge at $\alpha = 1$. The form of u_{rel} defined by eq.(3.2.2) is originally applicable to bubbly flow and not to annular flow regime ($\alpha > 0.8$). However, Schimizu and Asahi[5] have pointed out that by using the large value of $\alpha_c \approx 0.99$, the correlation given by eqs.(3.2.2) to (3.2.4) yields, in the reflooding stage, relative velocities similar to those used to in the RELAP4 code[16] which reflect the experimental air-water cocurrent and countercurrent bubbly flow data and transparent vessel air-water flooding data in the annular flow region. In the present calculation α_c is taken to be 0.98. In evaluating the quantites I, u_{gj} and u_{rel}, average values of the quanties x, α, ρ_{fs}, h_{gs}, h_{fs} and σ of the respective node are used.

The direction of drift flux is treated as below. All the combinations of two vertical or horizontal nodes are shown in Fig. 3.1, where the vertical and horizontal nodes are expressed by solid and dashed lines,

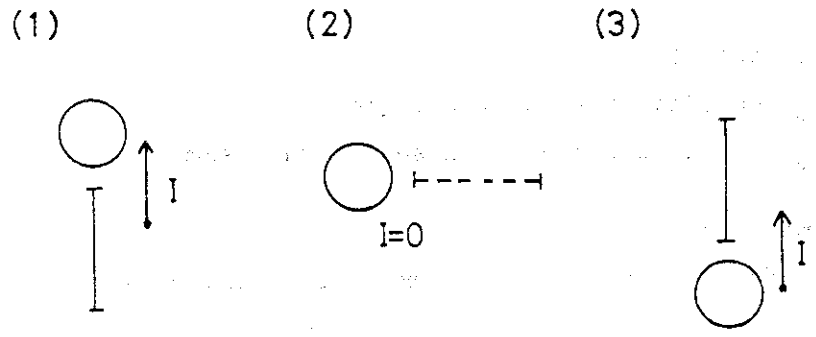

Fig. 3.1 Direction of Drift Enthalpy Flux for Normal Junction

respectively. Since the drift flux model is essentially applicable to the vertical nodes and not to horizontal ones, it is taken into account only in the cases of (1) and (4). In the case of (5), the drift flux model is not applyed since the drift flux from each side of normal junction is expected to cancel out. The direction of drift flux is assumed to be independent of the direction of mass velocity. The drift flux for mixing junction is also determined in the same manner as normal junction,

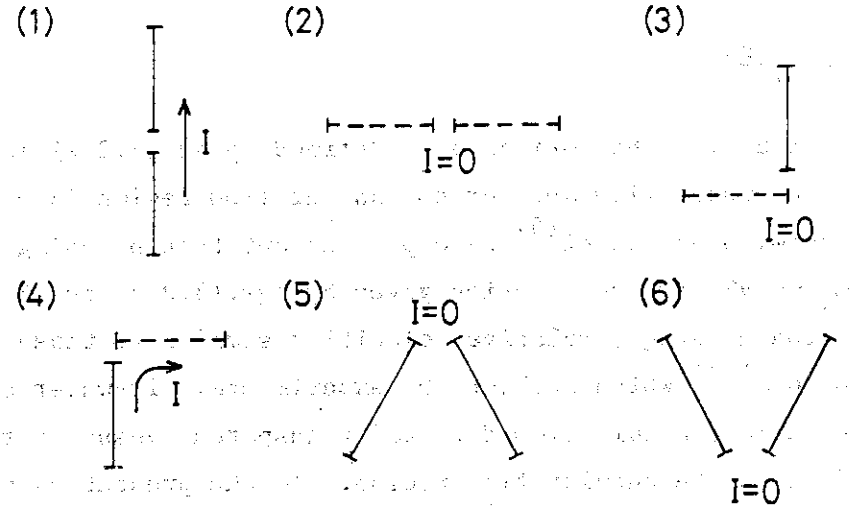

Fig. 3.2 Direction of Drift Enthalpy Flux for Mixing Junction

which is shown in Fig. 3.2.

3.3 Energy Equation

There are two kinds of junctions in the THYDE-P code: One is the normal or injection junction which is without volume and the other is

the mixing junction which is with volume. In the old version of the THYDE-P code, energy was not strictly conserved at normal and mixing junctions. This is due to the fact that during the short time after the flow direction of a node changed, the outgoing enthalpy did not strictly coincide with the enthalpy flowing into the adjacent node. When core nodes are quenching, a severe fluctuaction of mass flow occures at the core nodes. So for the present calculation, the code was modified so that energy conservation at normal and mixing junction holds strictly.

At first the energy conservation at normal node will be discussed below. As mass flow must be conserved in the normal junction we obtain

$$A_n \, G_n^E = A_{n'} \, G_{n'}^A \tag{3.3.1}$$

where A_n; flow area of node n

G_n^A ; mass flux at inlet point of node n

G_n^E ; mass flux at outlet point of node n

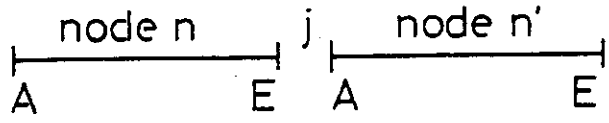

Fig. 3.3 Normal Junction in THYDE-P

Futhermore, with the use of $h_n^E = h_{n'}^A$, we obtain

$$A_n \, G_n^E \, h_n^E = A_{n'} \, G_{n'}^A \, h_{n'}^A \, . \tag{3.3.2}$$

We construct the drift enthalpy flow $\ell = A_n I_n$, where the quantity I_n have been defined by eq.(3.2.1),

so as to be $A_n \, I_n^E = A_{n'} \, I_{n'}^A$. (3.3.3)

Therefore we obtain

$$A_n \, \Lambda_n^E = A_{n'} \, \Lambda_{n'}^A \tag{3.3.4}$$

where Λ is the enthalpy flux defined by

$$\Lambda = Gh + I$$

It is apparent from eq.(3.3.4) that energy is strictly conserved at normal junction.

Secondly the code was modified so as to satisfy the energy conservation at mixing junction using continuity of enthalpy h, mass flux G and drift enthalpy flow ℓ, in the same as discussed above.

3.4 Phase Separation Model at Downcomer Top

In THYDE-P code, the specific enthalpy of the outgoing flows from the mixing junction is assumed to be equal to that of the mixing junction. The enthalpy of the mixing junction is calculated using the flowing equation

$$\frac{d}{dt}(\rho_j h_h^+) = (\sum_{j_f} A_n \Lambda_n^E - \sum_{j_t} A_n \Lambda_n^A)/V_j \quad , \tag{3.4.1}$$

where

ρ_j ; density of mixing junction

h_j^+ ; specific enthalpy of mixing junction

V_j ; volume of mixing junction

A_n ; cross section area of to − or from − node

Λ ; enthalpy flux of to − or from − node

and the summation $\sum_{j_f}$ is over the flows coming into the junction, while the summation $\sum_{j_t}$ is over the flows outgoing from the junction. Futher the homogeneous model is applied in the mixing junction. It should be noted, however, that there may be cases where the enthalpy of the outgoing flow is quite different from that of the mixing junction due to phase separation. For example, in the upper part of a pipe downcomer in PKL-facility (see Fig. 2.4), there are two incoming flows whose enthalpies are quite different. One is the flow with high enthalpy through the steam generators of the intact loops and the other is the flow of injected water with low enthalpy. Since the internals in the upper part (internal annular baffle structure) ensure that emergency cooling water cannot be bypassed directly to the broken loop, it may be reasonable to assume that vapor with high enthalpy flows out to the break and saturated liquid down to the downcomer pipe when flow becomes stagnant. These physical phenomena may be partly accounted for by using the drift flux model. It seems, however, that a model with very many nodes is needed in order to describe such phenomena only with the drift flux model.

In this report, the following simple model is tentatively adopted. We assume complete phase separation at the downcomer top in contrast

to the homogeneous model:

$$h_{out} = S(x)\, h_{fs} + (1 - S(x))\, h_{gs} \quad , \tag{3.4.2}$$

where

$$S(x) = \begin{cases} 1 & 0 \le x \le \tilde{x}_c \\ \exp(-\dfrac{x - \tilde{x}_c}{\Delta x}) & \tilde{x}_c \le x \le 1 \end{cases} \tag{3.4.3}$$

The smoothing function S(x) is introduced in order to eliminate the extreme enthalpy change of the mixing junction caused by mode change (see Fig. 3.4).

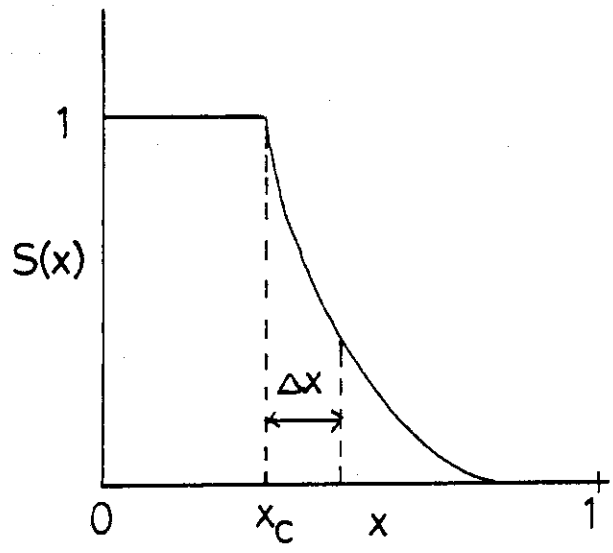

Fig. 3.4 Smoothing function S(x)

For the flows to the downcomer pipe (node 30) and to the break (node 29), we adopt $\tilde{x}_c$ = 0.9 and 0.1, respectively, along with Δx = 0.1.

3.5 Minimum Stable Film Boiling Temperature

The minimum stable film boiling temperature T_{MSFB} is the temperature of a wall which is required to maintain film boiling. The data support the phypothesis[19] that two mechanisms compete to determine T_{MSFB} in pool boiling. The first is the classic film boiling mechanism as originally analyzed by Berenson[17] and later modified by Henry[18] to include the effect of the thermal properties of the surface. The second mechanism is based on the phenomenon of homogeneous nucleation.

In the present model we adopt the following formula recommended by Bjormard and Griffith[19] for the homogeneous nucleation phenomena:

$$T_{MSFB} = T_{HN} + (T_{HN} - T_{\ell}) \left[(\rho\tilde{k}C_p)_{liquid}/(\rho\tilde{k}Cp)_{wall}\right]^{\frac{1}{2}} \qquad (3.5.1)$$

where

ρ ; density

$\tilde{k}$; thermal conductivity

Cp; specific heat capacity

T_{ℓ}; liquid temperature

and T_{HN} is the homogeneous nucleation temperature of a fluid at which nucleation will occur spontaneously in the liquid phase in the complete absence of preferred nucleon sites. It varies from 307°C at atmospheric pressure to the critical temperature (374°C) at the critical pressure for water. The value of T_{HN} is calculated assuming the following linear equation:

$$T_{HN}\ (°C) = 307 + 2.87\ (p\ (N/m^2) - 1.01 \times 10^5) \qquad (3.5.2)$$

where we take the values T_{HN} = 307 and 324°C[19] at $p = 1.01 \times 10^5$ and 6.89×10^5 (N/m^2), respectively. Under the conditions of this experiment, we obtain $T_{HN} \simeq 320°C$ and $T_{MSFB} \simeq 350°C$.

4. Preparation of Input Data

A nordalization scheme in the present calculation is shown in Fig. 4.1. Nodes from 1 to 14 and nodes from 15 to 29 form the intact and broken loops, respectively. The intact single and double loops are sumed up to one loop in the present analysis. The pressure vessel is expressed by an assembly of nodes from 30 to 46. The pipe-downcomer is expressed by a single node 30. The nodes from 32 to 45 are the core part, in which nodes 32 and 45 simulate the non-heated parts of the core. Nodes 31 and 46 are the lower and upper plenums, respectively. The upper head, pressure equalization line and annular gap are expressed by a single linkage node 48. The likage node 47 is the ECCS injection line. The special nodes 49 and 50 form the secondary sides of intact and broken loop steam generators, respectively. Axial power profile and temperature detector locations of PKL heater elements are shown in Fig. 4.2 with the corresponding nordalization. Futhermore, these heater rods are nordalized radially into 5 nodes, as shown in Fig. 4.3.

The input data used in the calculations are listed in app. A. The major parts of them are summarized in this section. The geometrical data and loss coefficients for each node are shown in Table 4.1 and 4.2, respectively.

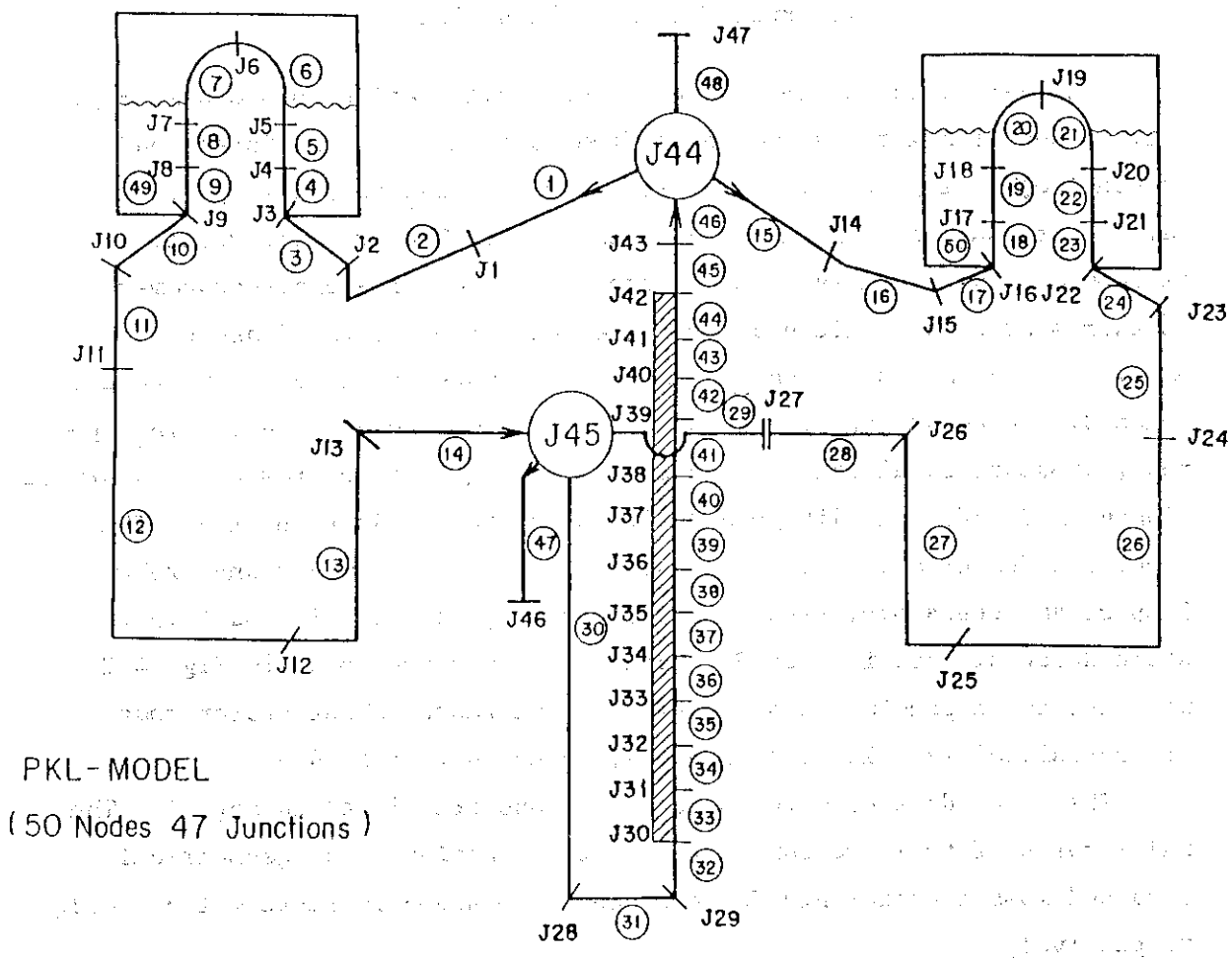

Fig. 4.1 Nordalization for PKL Test K9

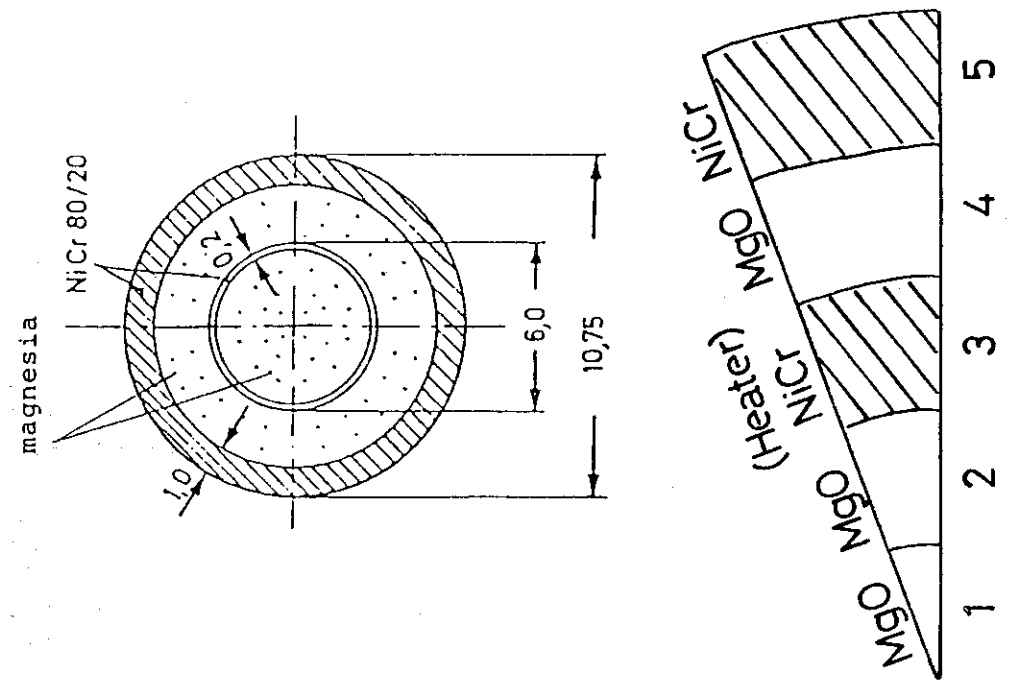

Fig. 4.3 Cross Section of Heater Element and its Nordalization

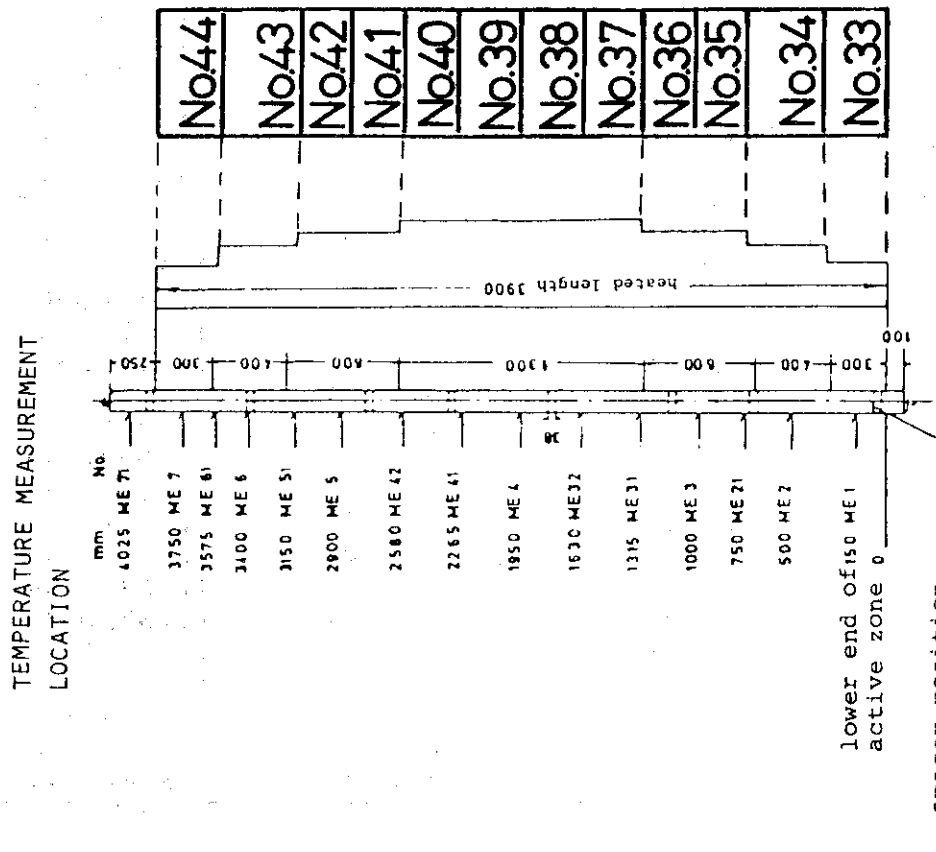

Fig. 4.2 Axial Power Profile and Temperature Measuring Positions of Heater Elements and its Nordalization

Table 4.1 Node Geometrical Data

Node No.	Description	Node Length L (m)	Node Height H_L (m)	Flow Area A (m^2)
1	DUCT NODE	3.035D+00	3.7100D-01	1.5174D-02
2	DUCT NODE	1.878D+00	1.6230D+00	3.6305D-02
3	S.G CHAMBER	2.560D-01	2.5600D-01	7.7931D-02
4	S.G PRIMARY	9.650D-01	9.6500D-01	2.8352D-04
5	S.G PRIMARY	9.650D-01	9.6500D-01	2.8352D-04
6	S.G PRIMARY	6.725D+00	6.5100D+00	2.8352D-04
7	S.G PRIMARY	4.725D+00	-4.5100D+00	2.8352D-04
8	S.G PRIMARY	3.000D+00	-3.0000D+00	2.8352D-04
9	S.G PRIMARY	9.300D-01	-9.3000D-01	2.8352D-04
10	S.G CHAMBER	2.560D-01	-2.5600D-01	7.7931D-02
11	DUCT NODE	1.836D+00	-1.6230D+00	3.6305D-02
12	DUCT NODE	5.322D+00	-3.9210D+00	1.5174D-02
13	PUMP NODE	3.445D+00	3.4450D+00	1.5174D-02
14	DUCT NODE	2.860D+00	2.5000D-01	1.5174D-02
15	DUCT NODE	2.503D+00	3.7100D-01	5.1275D-03
16	DUCT NODE	1.770D+00	1.6810D+00	1.2271D-02
17	S.G CHAMBER	1.980D-01	1.9800D-01	2.9864D-02
18	S.G PRIMARY	9.650D-01	9.6500D-01	2.8352D-04
19	S.G PRIMARY	9.650D-01	9.6500D-01	2.8352D-04
20	S.G PRIMARY	6.725D+00	6.5100D+00	2.8352D-04
21	S.G PRIMARY	4.725D+00	-4.5100D+00	2.8352D-04
22	S.G PRIMARY	3.000D+00	-3.0000D+00	2.8352D-04
23	S.G PRIMARY	9.300D-01	-9.3000D-01	2.8352D-04
24	S.G CHAMBER	1.980D-01	-1.9800D-01	2.9864D-02
25	DUCT NODE	1.738D+00	-1.6810D+00	1.2271D-02
26	DUCT NODE	5.370D+00	-3.8980D+00	5.1275D-03
27	PUMP NODE	3.457D+00	3.4570D+00	5.1275D-03
28	DUCT NODE	1.243D+00	2.1500D-01	5.1275D-03
29	DUCT NODE	1.028D+00	0.0	5.1275D-03
30	DOWN COMER	8.369D+00	-7.3340D+00	3.2365D-02
31	LOWER PLENUM	2.035D+00	1.2115D+00	1.4447D-01
32	CORE NODE	2.317D-01	1.6500D-01	1.1372D-04
33	CORE NODE	3.000D-01	3.0000D-01	1.1372D-04
34	CORE NODE	4.000D-01	4.0000D-01	1.1372D-04
35	CORE NODE	3.000D-01	3.0000D-01	1.1372D-04
36	CORE NODE	3.000D-01	3.0000D-01	1.1372D-04
37	CORE NODE	3.000D-01	3.0000D-01	1.1372D-04
38	CORE NODE	3.000D-01	3.0000D-01	1.1372D-04
39	CORE NODE	3.000D-01	3.0000D-01	1.1372D-04
40	CORE NODE	4.000D-01	4.0000D-01	1.1372D-04
41	CORE NODE	3.000D-01	3.0000D-01	1.1372D-04
42	CORE NODE	3.000D-01	3.0000D-01	1.1372D-04
43	CORE NODE	4.000D-01	4.0000D-01	1.1372D-04
44	CORE NODE	3.000D-01	3.0000D-01	1.1372D-04
45	CORE NODE	2.823D-01	2.5000D-01	1.1372D-04
46	UPPER PLENUM	1.600D+00	1.6625D+00	1.1937D-01
47	ECCS PIPING	2.000D+00	-1.0000D+00	1.5174D-02
48	ANNULAR GAP	1.043D+01	-6.7630D+00	7.3488D-02

Table 4.2 Loss Coefficients

Node. NO.	k	k_A^f	k_A^r	k_E^f	k_A^f
1	0.702	0.5	1.0	0.0	0.0
2	0.21	0.887	0.0572	0.0	0.0
3	0.0	2.48	1.83	3.38	9.52
4	0.691	0.0	0.0	0.0	0.0
5	0.691	0.0	0.0	0.0	0.0
6	0.402	0.0	0.0	0.0	0.0
7	0.0	0.0	0.0	0.0	0.0
8	0.394	0.0	0.0	0.0	0.0
9	0.7φ9	0.0	0.0	0.0	0.0
10	0.0	9.52	3.38	1.83	2.48
11	0.157	0.0	0.0	0.0572	0.887
12	2.19	0.0	0.0	0.0	0.0
13	0.496	0.0	0.0	0.0	0.0
14	1.76	0.0	0.0	1.0	0.5
15	0.697	0.5	1.0	0.0	0.0
16	0.183	0.756	0.0573	0.0	0.0
17	0.0	3.59	2.37	4.44	12.3
18	0.484	0.0	0.0	0.0	0.0
19	0.484	0.0	0.0	0.0	0.0
20	0.402	0.0	0.0	0.0	0.0
21	0.471	0.0	0.0	0.0	0.0
22	0.394	0.0	0.0	0.0	0.0
23	0.502	0.0	0.0	0.0	0.0
24	0.0	12.3	4.44	2.37	3.59
25	0.155	0.0	0.0	0.0573	0.756
26	2.23	0.0	0.0	0.0	0.0
27	34.348	0.0	0.0	0.0	0.0
28	1.53	0.0	0.0	1.0	1.0
29	0.0	1.0	1.0	100.0	1.0
30	0.771	0.3724	0.685	1.0	0.5
31	0.0	0.0	0.0	0.0	0.0
32	0.813	8.68	8.9	0.0	0.0
33	0.755	0.0	0.0	0.0	0.0
34	0.67	0.0	0.0	0.0	0.0
35	0.755	0.0	0.0	0.0	0.0
36	0.755	0.0	0.0	0.0	0.0
37	0.755	0.0	0.0	0.0	0.0
38	0.755	0.0	0.0	0.0	0.0
39	0.755	0.0	0.0	0.0	0.0
40	0.67	0.0	0.0	0.0	0.0
41	0.755	0.0	0.0	0.0	0.0
42	0.755	0.0	0.0	0.0	0.0
43	0.67	0.0	0.0	0.0	0.0
44	0.755	0.0	0.0	0.0	0.0
45	0.77	0.0	0.0	3.98	2.99
46	0.0	0.0	0.0	0.0	0.0
47	0.0	0.0	0.0	0.0	0.0
48	2.5	1.5	1.5	0.0	0.0

4.1 Core Data

The core power history has previously been listed in Table 2.1 and 2.2.

Input data for the core nodes are:

Number of heater rods	337
Outer diameter of heater rods	5.375×10^{-3} (m)
Rod pith	1.43×10^{-2} (m)

Initial heat flux

Node NO.	Heat flux (kcal/m^2sec)
32	non-heated
33	3.94
34	5.30
35	6.41
36	6.41
37	7.22
38	7.22
39	7.22
40	7.22
41	6.41
42	6.41
43	5.30
44	3.94
45	non-heated

Density of Magnesia	3150 Kg/m^3
Density of NiCr 80/20	8300 Kg/m^3

Specific heat capacity of MgO

θ (°C)	100	300	500	1000	1300
Cp (Kcal/Kg K)	0.2483	0.2782	0.2916	0.3102	0.3186

Specific heat capacity of NiCr 80/20 0.12 Kcal/Kg K independent of temperature

Thermal conductivity of MgO

θ (°C)	100	300	500	700	900	1100
k (Kcal/sec·m·K) $\times 10^{-3}$	4.78	3.25	1.94	1.36	1.10	1.03

Thermal conductivity of NiCr 80/20

θ (°C)	20	250	550	800	1300
k (Kcal/sec m K) $\times 10^{-3}$	2.87	3.90	5.11	6.12	8.08

4.2 Steam Generator Data

The primary and secondary systems of the steam generator in the broken loop are simulated by nodes from 17 to 24 and mode 50, respectively. Nodes 17 and 24 are the inlet and outlet chamber, respectively. Nodes from 18 to 23 simulate the primary coolant in the U-tubes. Nodes from 3 to 10 and node 49 form the steam generators in both single and double intact loops of PKL-facility. The input data for these nodes are:

		broken loop	intact loop
U-tubes			
Number of U-tubes		30	90
Inner diameter	(m)	9.5×10^{-3}	9.5×10^{-3}
Height	(m)	8.43	8.43
Pitch	(m)	3.64×10^{-2}	3.42×10^{-2}
Secondary system			
Pressure	(atm)	54.04	56.59
Feed water enthalpy	(Kcal/Kg)	273.7	273.7
Feed water mass flow rate	(Kg/sec)	3.8	9.6
Volume	(m^3)	0.5352	1.366
Height	(m)	8.576	8.586
Cross section	(m^2)	6.24×10^{-2}	1.59×10^{-1}
Subcooled water level	(m)	4.2	4.2
Void fraction of saturated region		0.99	0.99

Initial heat flux for the fictions blowdown

Node NO.	Heat flux (Kcal/m^2sec)
Intact loop	
4	2.0
5	2.0
6	1.8
7	1.8
8	1.9
9	1.9
Broken loop	
18	2.0
19	2.0
20	1.8
21	1.8
22	1.9
23	1.9

The time for feed water shut down is 0.4 sec. after the break.

4.3 Pump Data

The PKL test facility does not include a pump. However, it is presumed in the THYDE-P steady state adjustment. IN THYDE-P, a pump node is a variation of a normal node with a pump head. In the present calculation, the pump head is assumed to be

$$H(t) = Ho \exp(-\alpha t) \quad , \tag{4.1}$$

where

Ho ; pump head determind by steady state adjustment

t ; time after the break

$\alpha = 0.1 \ (sec^{-1})$

On this assumption, we obtain $H \approx 0$ at the test initiation.

4.4 ECCS Data

In the experiment, water was injected into both the single and double intact loops through nozzles. In addition, water was injected straight into the top of the downcomer on the same elevation as the reactor primary loops (see Figs 2.2 and 2.4). However, ECC water is assumed to be injected into a single junction 46 in the present calculations. The mass flow rate consistent with the experimental data is used, which is listed in Table 4.3. In the present calculation, injection starts at 35 sec. after the break, corresponding to the test initiation.

Table 4.3 Total Injection Rate

Time (sec)	0	1.5	5.0	10.2	17.6	24.9	26.0	350.0
Flow Rate (Kg/sec)	22.0	22.3	20.3	17.5	14.8	13.0	1.9	1.9

4.5 Break Data

The double ended break is assumed to occur at junction 27. The break pressure is given to be consistent with the experimental data (see Fig. 2.5). When a reverse flow is calculated at the break point, the enthalpy of the coolant which flows into the system, can not be determined realistically because of a lack of a discharge tank model. In the present analysis, the coolant enthalpy for the reverse flow is obtained assuming quality $x = 0.9$. This rough approximation may be adequate in this case because the period of the reverse flow is short (about 30 sec.) and because the amount of mass flow into the system through the break point is rather small compared with that of injected ECC water.

5. Calculated Results and Discussion

The calculated results will be compared with the experimental data in this section. At first the detailed comparison between the calculated results and the individual experimental plots will be made in the following subsections. Secondly effects of the phase separation at the downcomer top will be investigated using a simple model. Finally we will show the improverment of the quench front curve obtained by taking account of the minimum stable film boiling temperature.

5.1 Cladding Surface Temperatures and Heat Transfer Coefficients

The calculational results of cladding surface temperatures at the measuring elevations (ME1 to ME7) are compared with the experimental results in Figs. 5.1 to 5.7, respectively. The experimental results are shown by a scatter field of the measured values for different rods at the same elevation. Two calculational results labelded by ME301 (node 35) and ME302 (node 36) are presented in Fig. 5.3 because the measuring position ME3 is located at the intermediate elevation between node 35 and 36 (see Fig. 4.2). Also in Figs 5.4 and 5.5, two results are shown, in the same way as Fig. 5.3.

Before considering the individual numerical results more in detail, a brief overview on the results will be given. The end of refill time that means the time when the ECC water enters the heated region of the heater rods in the core was well predicted by the calculations. The safety relevant maximum cladding surface temperature (677°C) was measured somewhat above the middle of the heated length after 82 sec. The maximum temperature is well reproduced by the THYDE-P code (about 660°C). However, the calculational results for the time when the maximum temperature occurs is considerably different from the experimental value. In addition to the maximum temperature, the residence time (during this time high temperature is existent) are somewhat influencing the oxidation process and the deformations of the cladding tubes in the reactor cores. The residence time above 590°C is largely underestimated by the calculation.

In addition to numerical values for the maximum cladding surface temperature and the maximum quenching time, the cladding temperature histories up to quenching are also important. Of cource, they are in

direct relation with the htc's.

Beginning with the lower powered ME1 and ME2, it is seen that initial surface temperatures are higher by about 100°C than the experimental values. But the behavior of the cladding temperature histories is well predicted by the calculation. The scatter field of the measured values is relatively small.

As for the refill and reflood processes, the typical history of the cladding surface temperature in the middle of the rods is devided into 5 phases as follows[5]:

Phase 1. The cladding temperature increases quickly caused by poor vapor cooling during the refill period.

Phase 2. The cladding temperature increases much slowlier immediatly after the beginning of reflood up to the turn-around point, due to higher steam production and water entrainment.

Phase 3. The cladding temperature decreases by continuously improved heat transfer due to such as rise of the oscillating water level with increased water entrainment and local film boiling.

Phase 4. The cladding temperature decreases increasingly faster due to film cooling and transition boiling.

Phase 5. Finally the cladding temperature is quenched down to the saturation temperature.

The comparison between calculated and experimental results is shown in Fig. 5.4. The calculated initial temperature increase and steep temperature drop during the quench are in good agreement with the experiment. It is however apparent that the experimental history of phases 2 and 3 is not reproduced. The calculational results show rapid decreasing temperature after the beginning of reflood without slow increase (phase 2). The same tendency is observed in the calculational results at ME3 and ME5 though not so remarkable.

The calculated histories of heat transfer coefficients are shown in Figs. 5.8 to 5.14, along with the experimental data. The temperature histories are directly dependent on the htc histories. Similar to all other ME, three levels of htc can be realized from the experimental data (see Fig. 5.11). During the refill phase, the htc has an average of about 10W/(m^2K), after that till quenching about 100W/(m^2K) and shortly after quenching (2700 ± 300) W/(m^2K). It is found that the calculated results after the beginning of reflood (rapidly decreasing temperature) correspond to the overestimation of the htc's by two or

three times.

5.2 Quench Fronts

Experimentally observed the quench fronts propagate from the both ends, bottom and top, into the core. The former by the ECC water flowing through the lower plenum to the rod bundle and the latter by the water, which is entrained by the vapor produced in the lower part of the rod bundle and then deentrained in the upper plenum. In the test the lower quench front propagation is slightly faster than the upper one. Figure 5.15 shows the comparison between the calculational and experimental results. In the analysis the lower quench front propagation is calculated by the mode change of heat transfer from mode 4.3 (pool film boiling) to mode 4.4 (pool transition boiling) due to the ECC water flowing through the lower plenum. On the other hand the quenching in the upper part of the rod bundle occurs when the cladding surface temperature decreases below the minimum film boiling temperature (mode 4.5). Although the slightly faster quenching is obtained in the middel part of the rod bundle, the calculated curve of the quench fronts is in good agreement with the experiment.

5.3 Differential Pressures

Pressure differences between downcomer nozzle region and break (DPRRC) and between upper plenum and break (DPOPC) are calculated and compared with the experimental data in Figs. 5.16 and 5.17, respectively.

From the stationary initial value these pressure differences drop down very rapidly because vapor in the primary system condensates at the cold injection water in the downcomer nozzle region and in the intact loops. This vapor is supplied from the intact loops, pressure vessel and mainly from the containment through the break. Shortly after reflood begins, the pressure difference increases very rapidly caused by vapor production and increased pressure losses. The vapor streaming from the containment is finished slowly and then the flow reverses, now directed to the break. Later on the pressure difference increases slowlier indicating the increasing pressure losses in the steam generator and mainly in high pump resistance. These experimental behaviors are well reproduced by the calculation except for three respects:

(1) The calculated pressure drop due to vapor condensation is about twice as large as the experiment, suggesting the inappropriate value of the delay parameter τ_D in a non-equilibrium model.

(2) The time when the system pressure increases very rapidly is about ten minutes late.

(3) The calculated pressure differences of DPRRC and DPOPC after the beginning of reflood are by 0.15 bar larger than the experimental data.

5.4 Mass Flow Rate

Except during refill, measured curves for mass flow rate in all loops show nearly the same character: Shortly after the beginning of reflood, the mass flow rates increase steeply and then increase slowly till about 160 sec. From that time on, they still increase slowlier up to a more or less stationary maximum value. These are closely related to the pressure difference between the pressure vessel and the break. Mass flow rate in the broken loop is in excellent agreement with the experiment as shown in Fig. 5.18. Deviation from the experimental value appears in the same respects as in the pressure differences discussed in subsec. 5.3.

Experimental mass flow rate in the intact single and double loops is unable to be compared directly with the calculational results, because the intact loops are sumed up to one loop in the present calculation. However, the calculated mass flow rate in the intact loop is in good agreement with the sum of the mass flow rate in the experimental intact single and double loops.

As for mass flow rate in downcomer-tube, the experiment shows at first a high negative value (see Fig. 5.19). After the mean flow rate is zero it becomes positive (directed to the pressure vessel) and increases to a stationary value of about 2.3 Kg/sec. from 160 sec. on. Oscillations caused by U-tube system (downcomer and pressure vessel) are seen in the experimental curve. In the present calculation downcomer-tube is simulated by a single node and its mass flow rate is assumed to be an average of those at the upper and lower ends. Because mass flow rates at the upper and lower ends of the downcomer-tube are quite different, it does not seem instructive to compare the calculated mean mass flow rate with the experiment. It is desirable to simulate the

downcomer-tube by several nodes.

5.5 Phase Separation Effects at the Downcomer Top

In the upper part of a pipe downcomer in PKL-facility, the phase separation is expected to occur when the flow becomes stagnant as has been discussed in subsect. 3.4. In this subsection we will examine the phase separation effects at the downcomer top.

The calculated results of the cladding surface temperatures and quench fronts without the phase separation model at the downcomer top are compared with the experimental results in Figs. 5.20 to 5.23. It is found that the quenching time at the higher measuring elevations (ME 5 to ME7) is considerably delayed. In order to investigate the reason why this delay occurs, the calculated results of the water level in the downcomer-tube with and without the phase separation model are compared with the experiment in Fig. 5.24, since the water level in the downcomer has a considerable influence on the quench front propagation. The water level in the downcomer decreases after 50 sec. when the phase separation is not taken into account. The reason is easily understood from Fig. 5.25, where the mass flux at the downcomer top is shown. The calculated curve of the mass flux flowing into the downcomer-tube decreases after the reflood begins and becomes almost zero, when the phase separation model is not included. This underestimation of the mass flux corresponds to the overestimation of the mass flow rate at the break compared with the experimental data (see Fig. 5.26). If the phase separation model is taken into account, the flow with high enthalpy goes out to the break as shown in Fig. 5.27. This seems to cause the reduction of the mass flow rate at the break.

5.6 Effects of Minimum Stable Film Boiling Temperature

When will examine the influences of the minimum stable film boiling temperature (MSFBT) on the histories of the cladding surface temperatures at the higher measuring elevations and the quench fronts. The calculated results of the cladding surface temperatures without the MSFBT model are compared with the experimental results in Fig. 5.28 to 5.31. In this case the quenching time at the higher elevations (ME5 to ME7) is considerably delayed because the quenching is caused only when the quality of a core node under consideration decreases below 0.1. If the MSFBT

model is taken into account, the quenching occurs when the cladding surface temperature decreases below 350°C, since T_{MSFB} is about 350°C under the conditions of this experiment. This improves the calculated results for the histories of the cladding surface temperatures at the higher elevations and the quench fronts, as has been shown in Figs. 5.1 to 5.7 and 5.15.

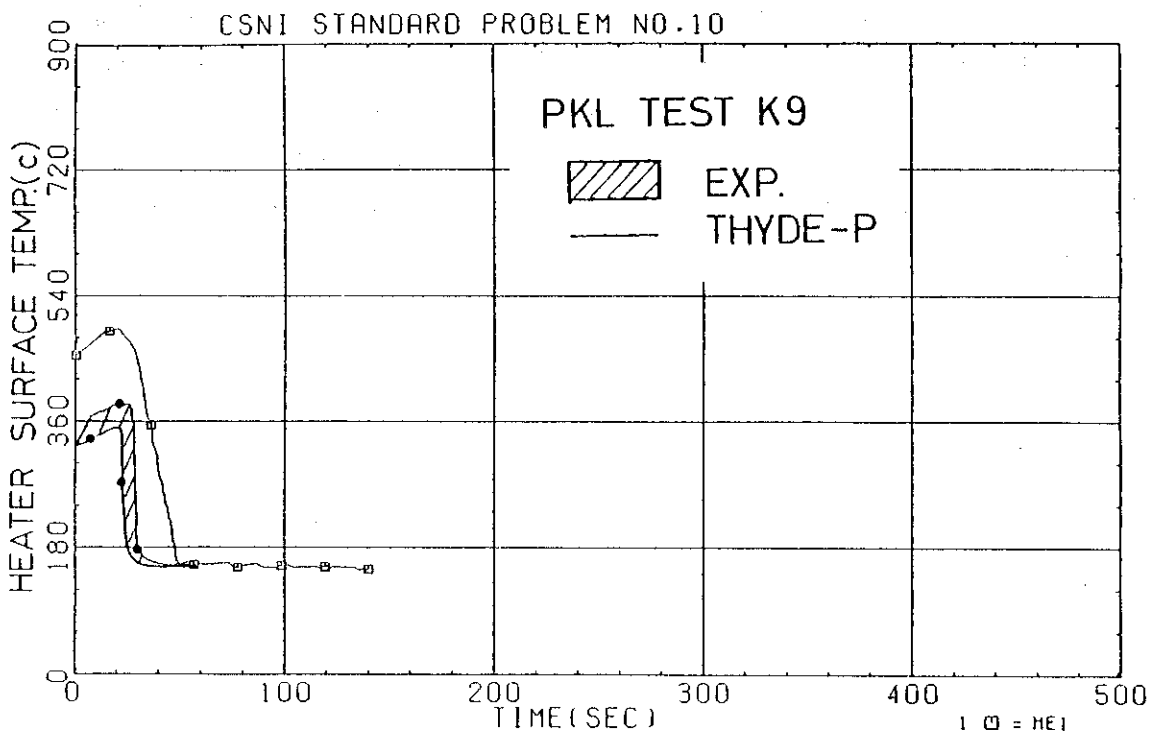

Fig. 5.1 Cladding Surface Temperatures (Elevation ME1)

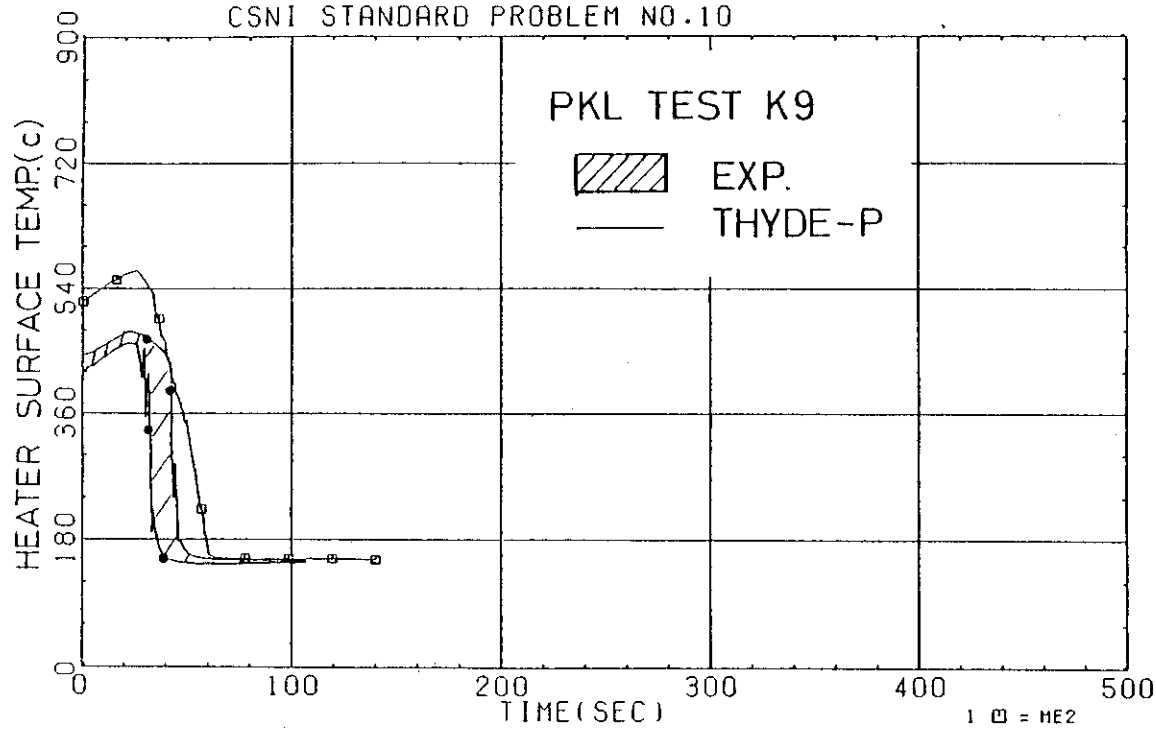

Fig. 5.2 Cladding Surface Temperatures (Elevation ME2)

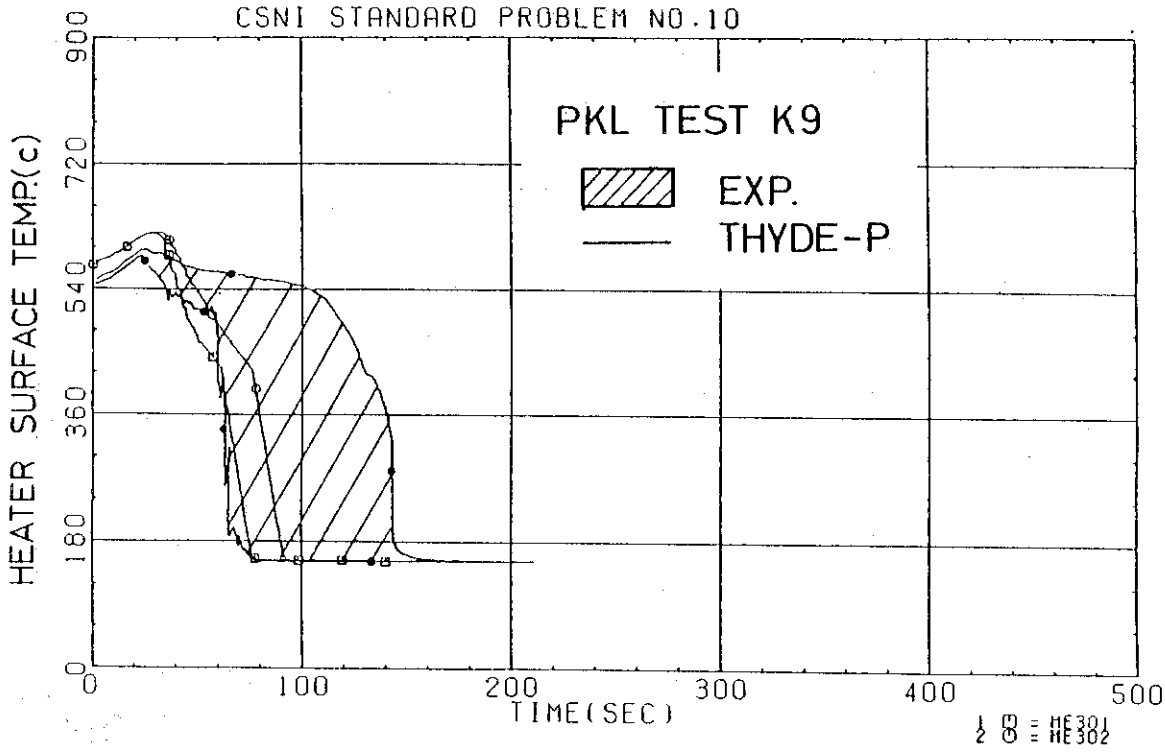

Fig. 5.3 Cladding Surface Temperatures (Elevation ME3)

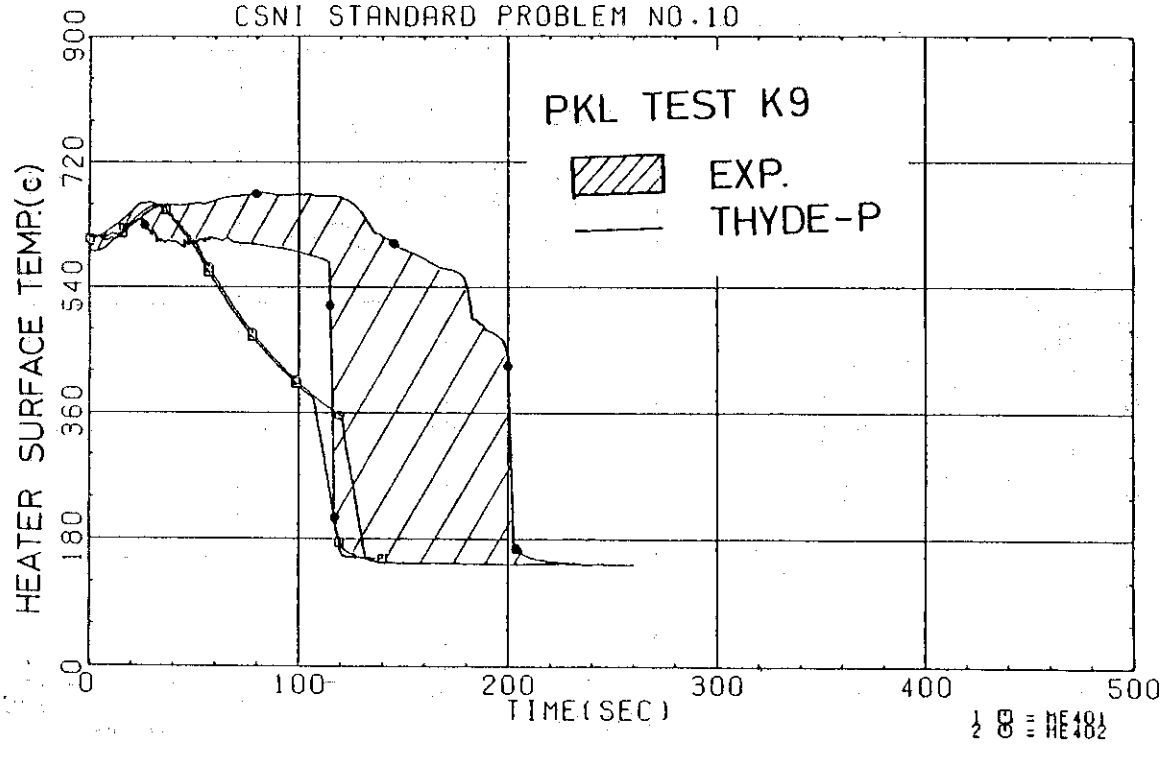

Fig. 5.4 Cladding Surface Temperatures (Elevation ME4)

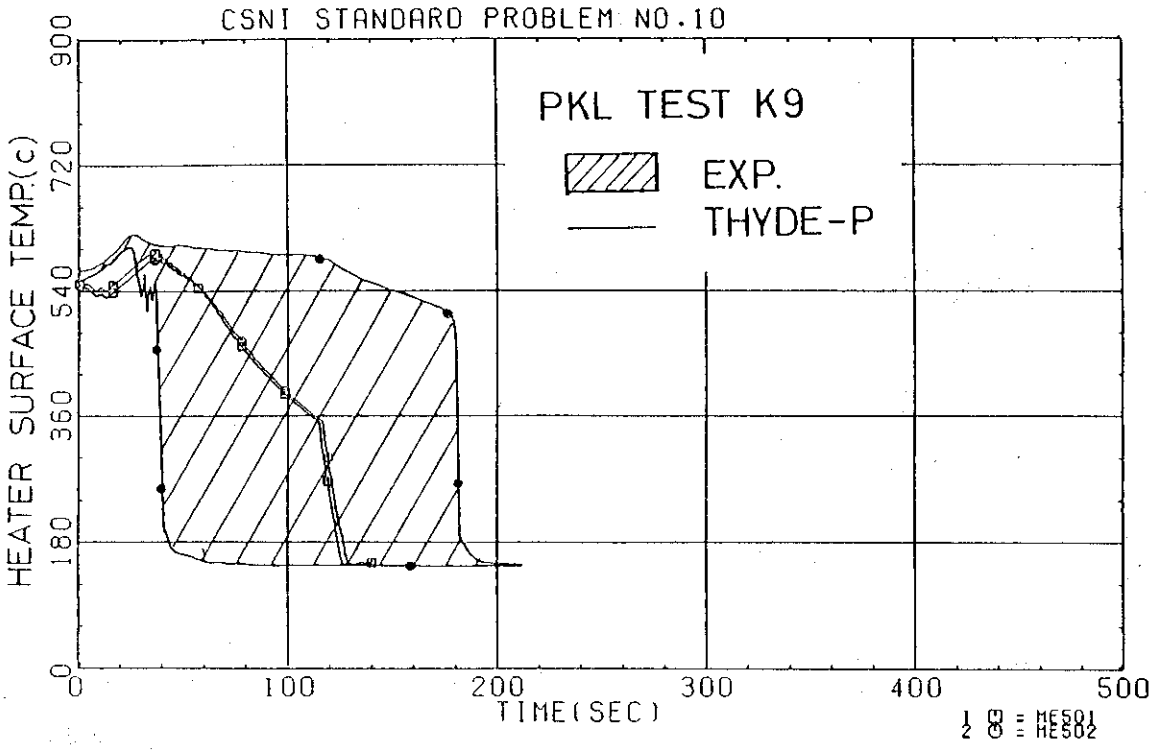

Fig. 5.5 Cladding Surface Temperatures (Elevation ME5)

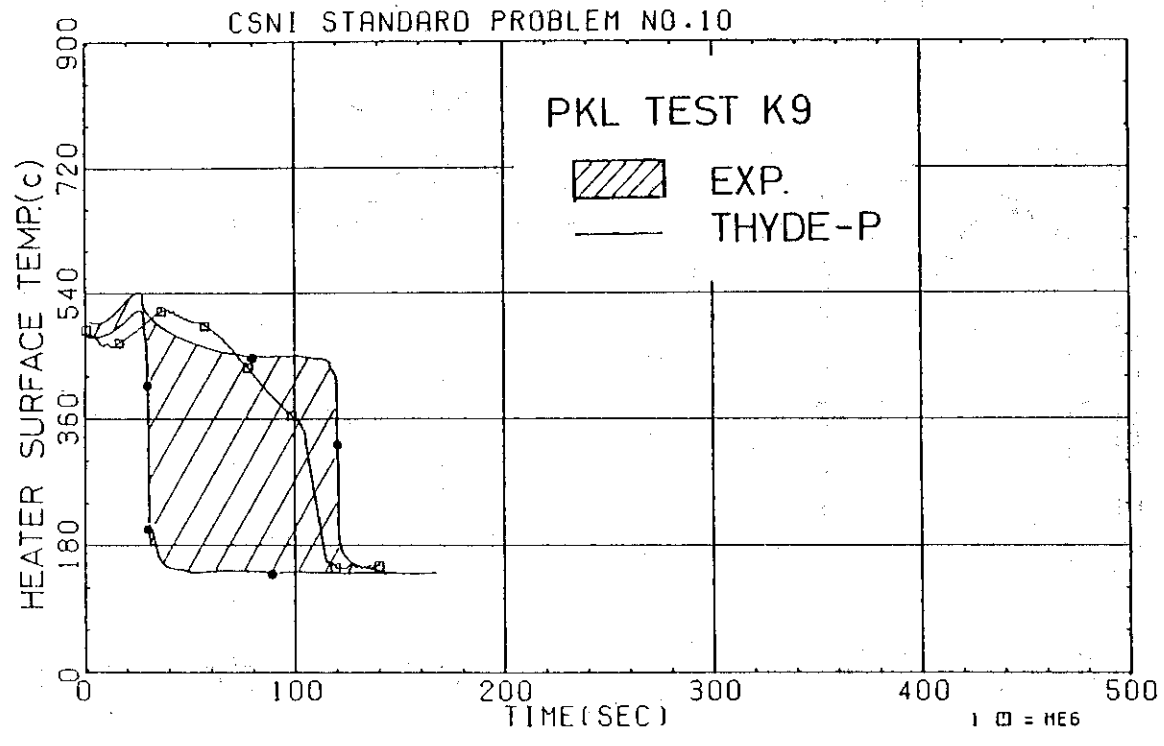

Fig. 5.6 Cladding Surface Temperatures (Elevation ME6)

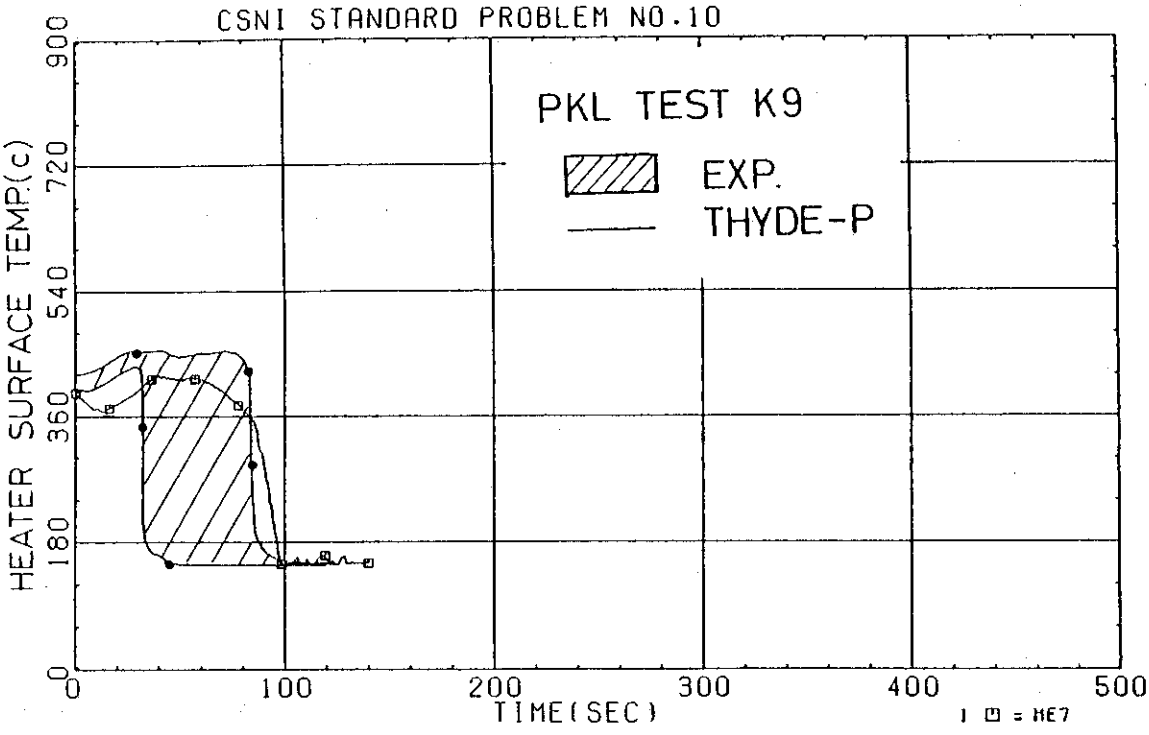

Fig. 5.7 Cladding Surface Temperatures (Elevation ME7)

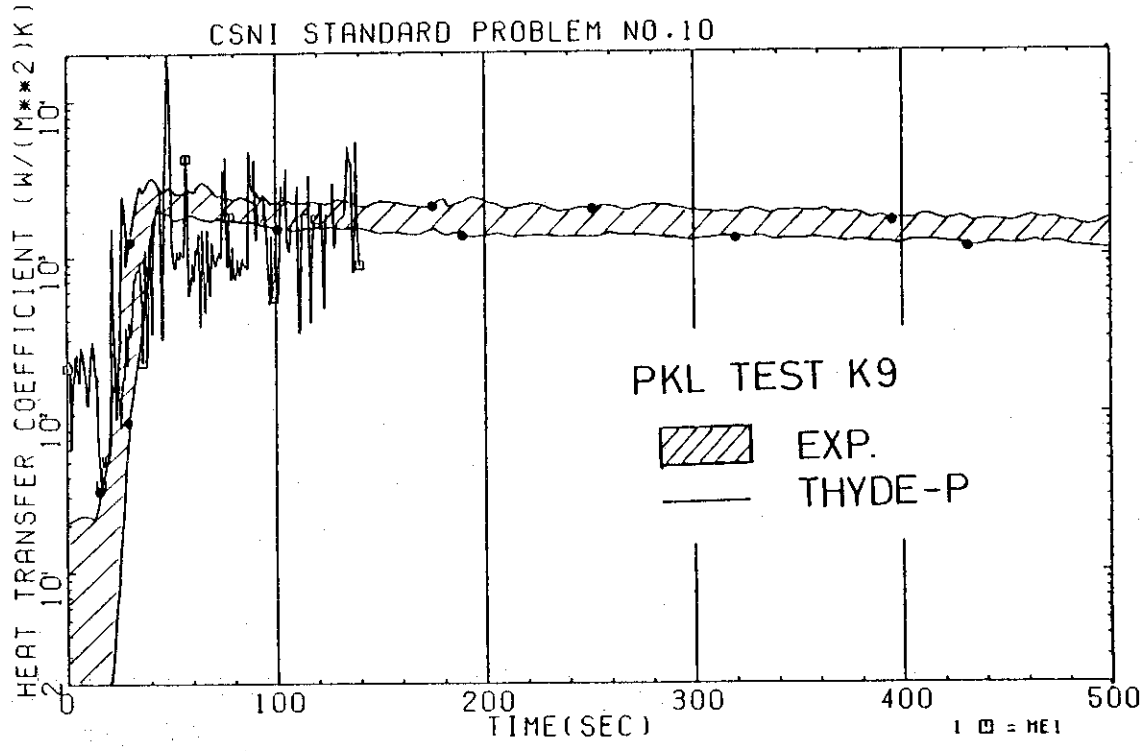

Fig. 5.8 Heat Transfer Coefficients (Elevation ME1)

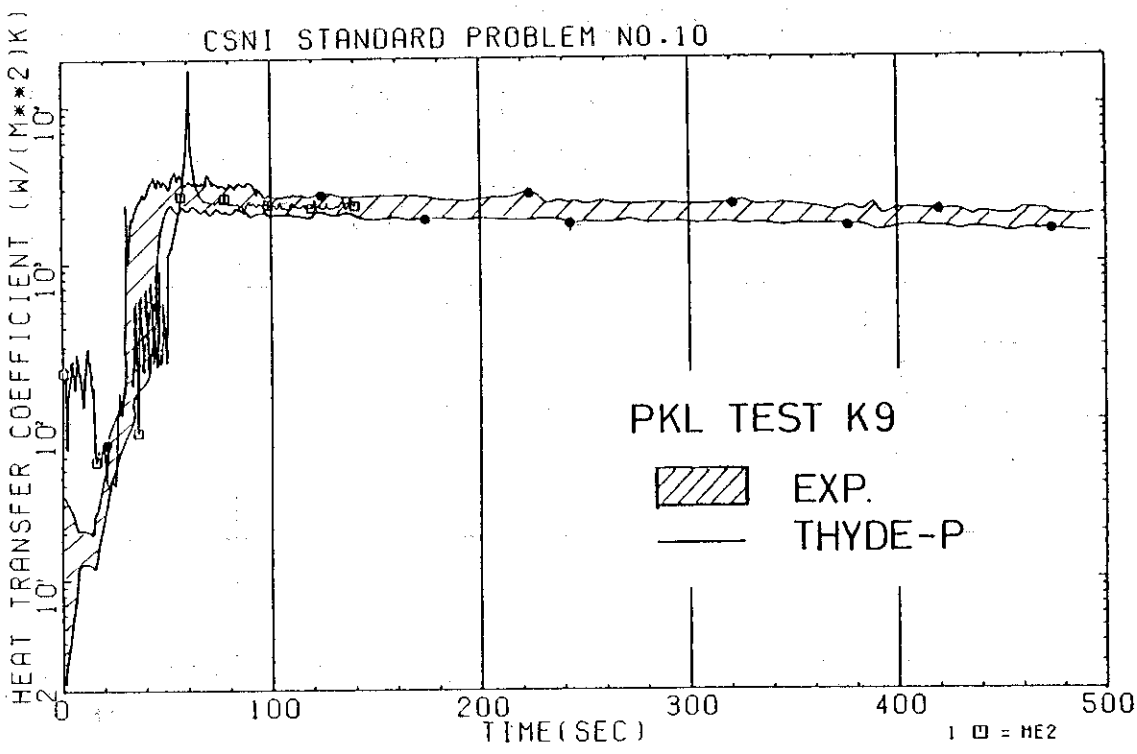

Fig. 5.9 Heat Transfer Coefficients (Elevation ME2)

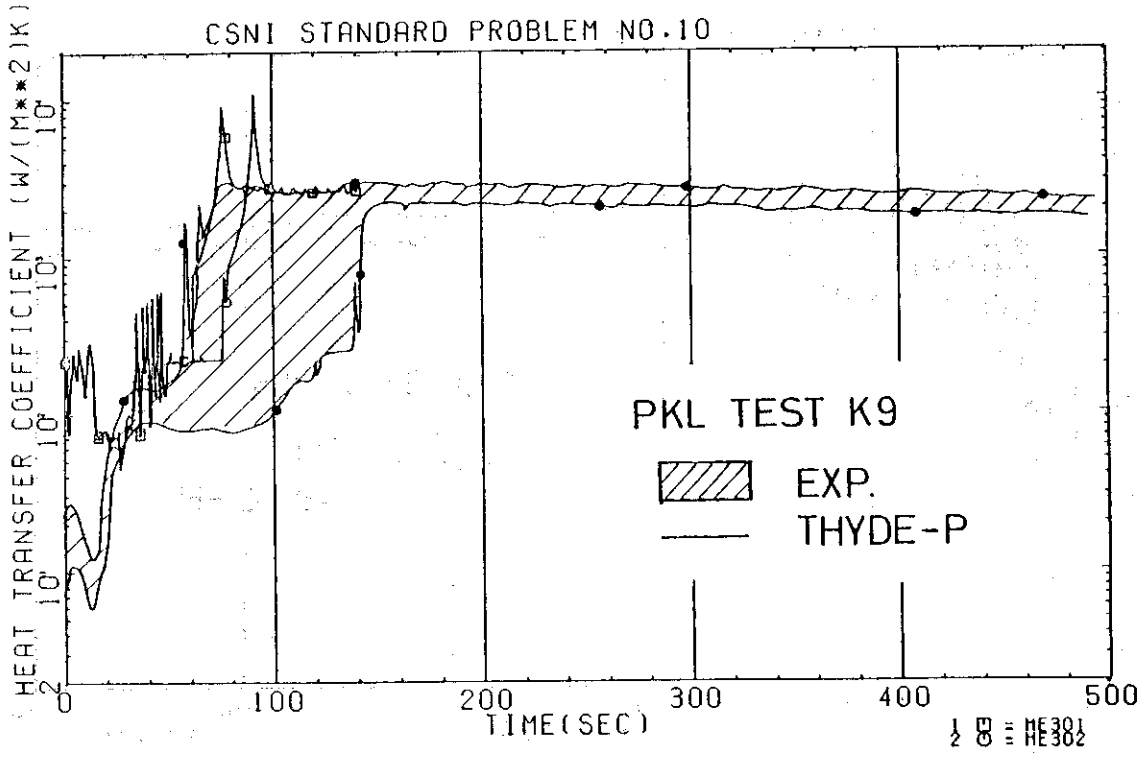

Fig. 5.10 Heat Transfer Coefficients (Elevation ME3)

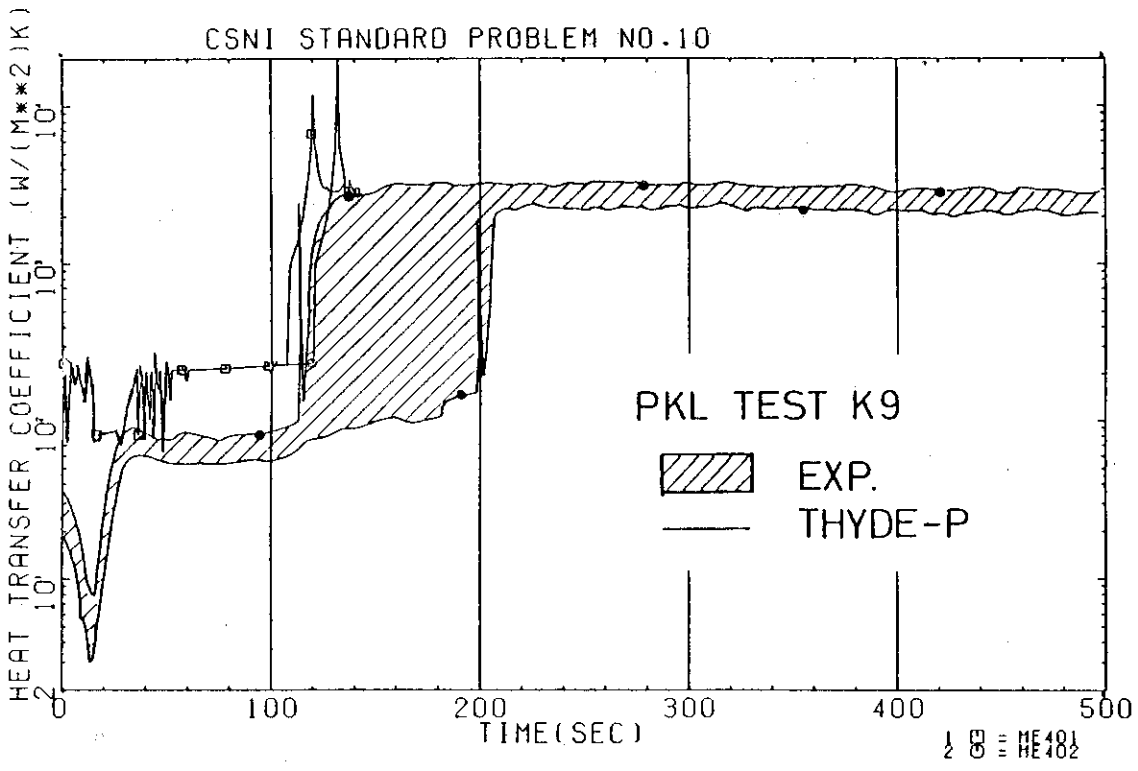

Fig. 5.11 Heat Transfer Coefficients (Elevation ME4)

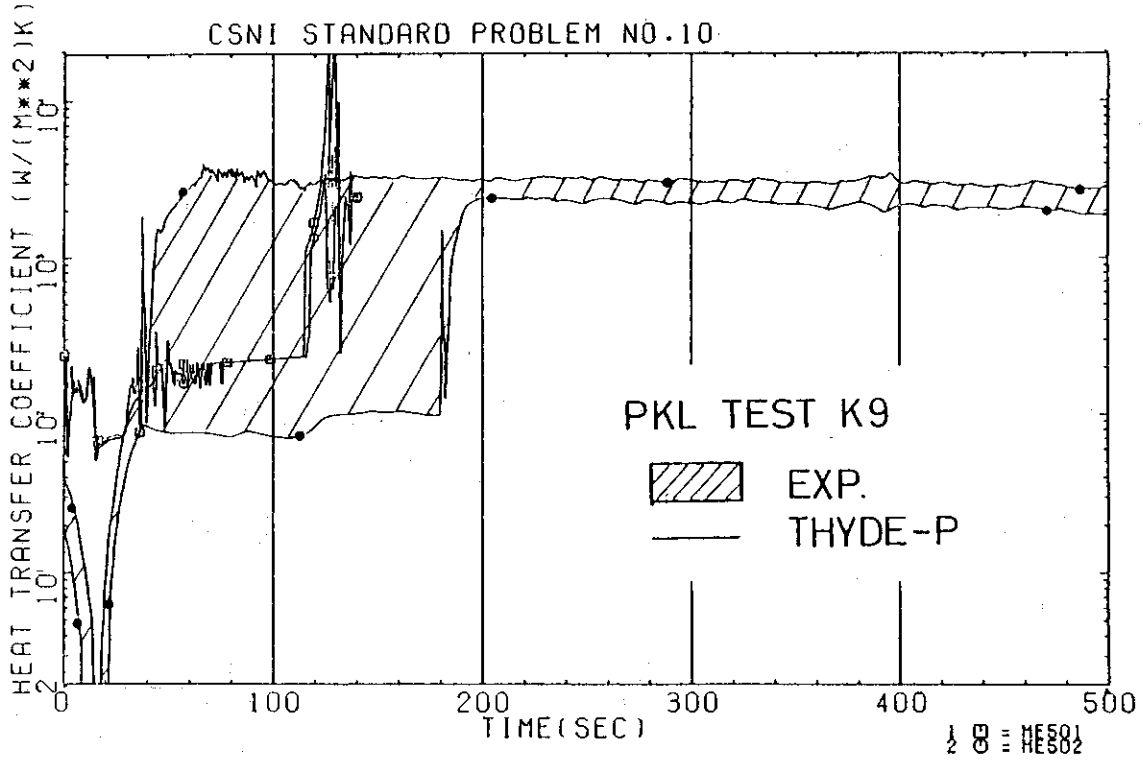

Fig. 5.12 Heat Transfer Coefficients (Elevation ME5)

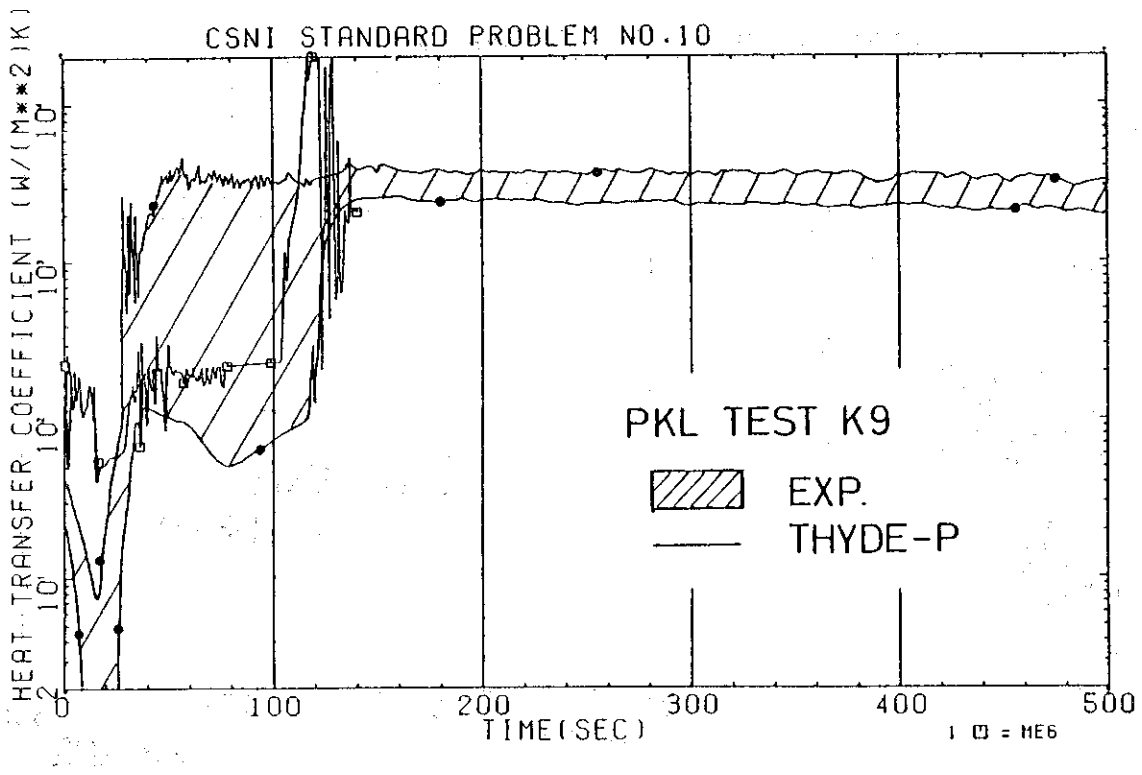

Fig. 5.13 Heat Transfer Coefficients (Elevation ME6)

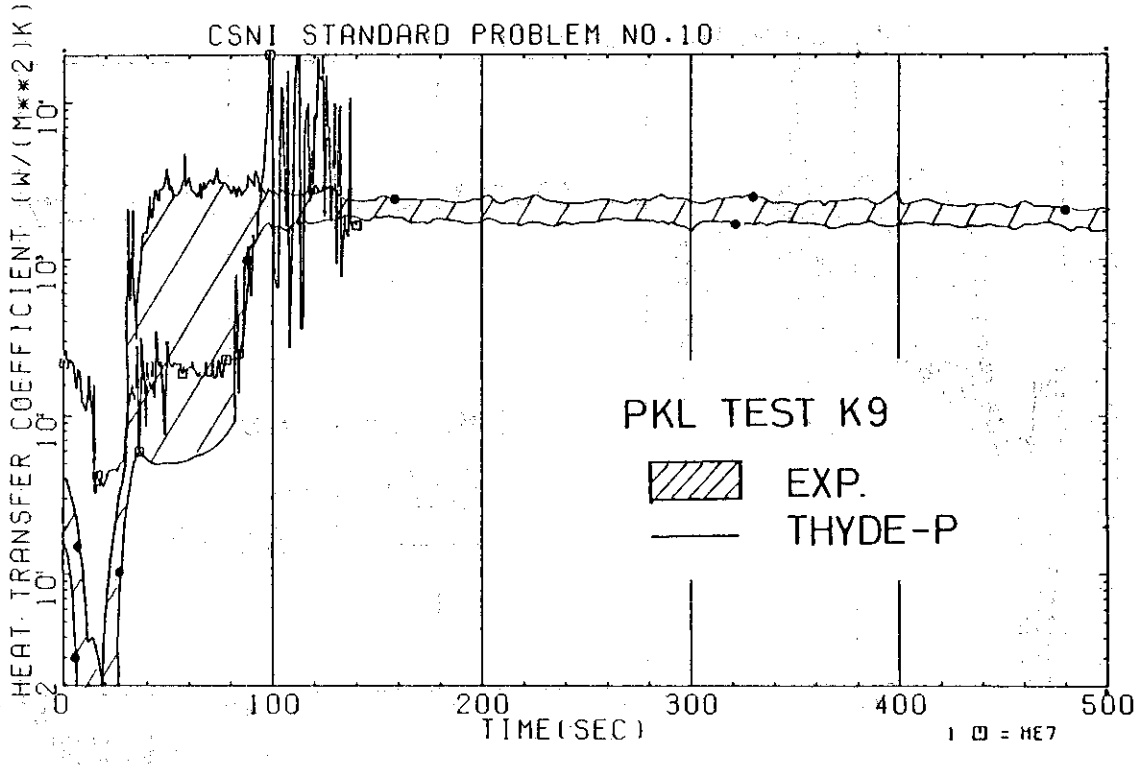

Fig. 5.14 Heat Transfer Coefficients (Elevation ME7)

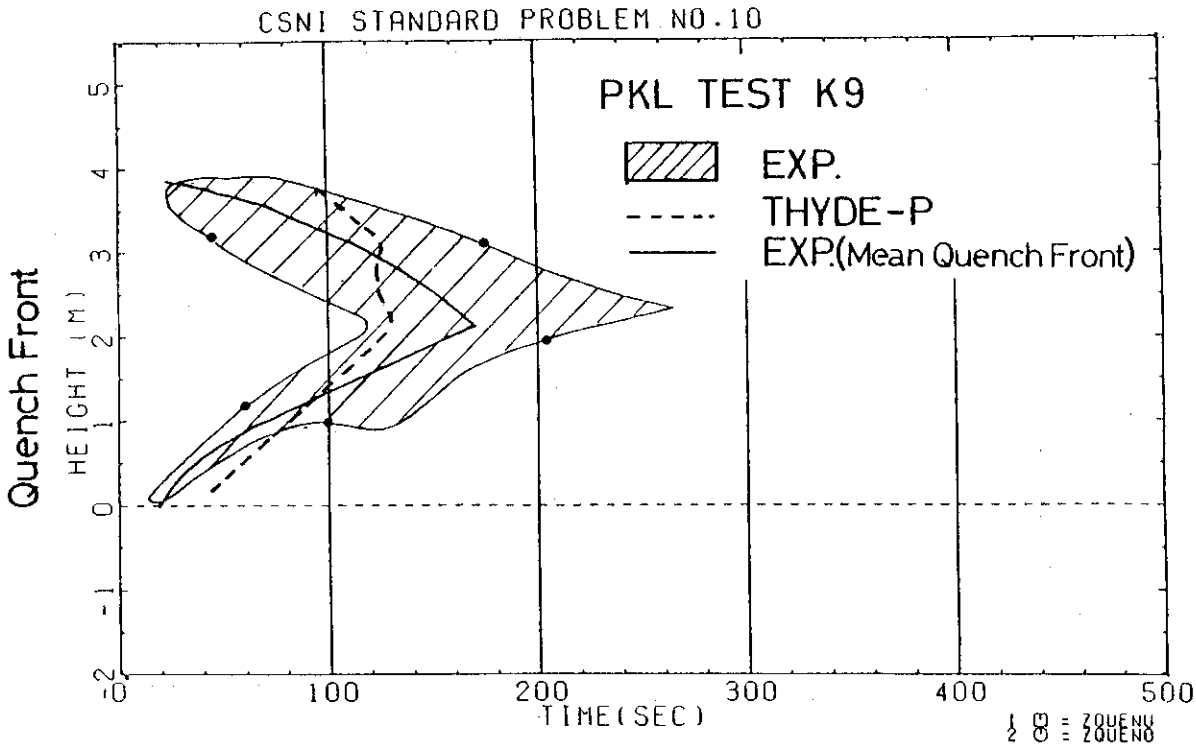

Fig. 5.15 Upper and Lower Quench Fronts

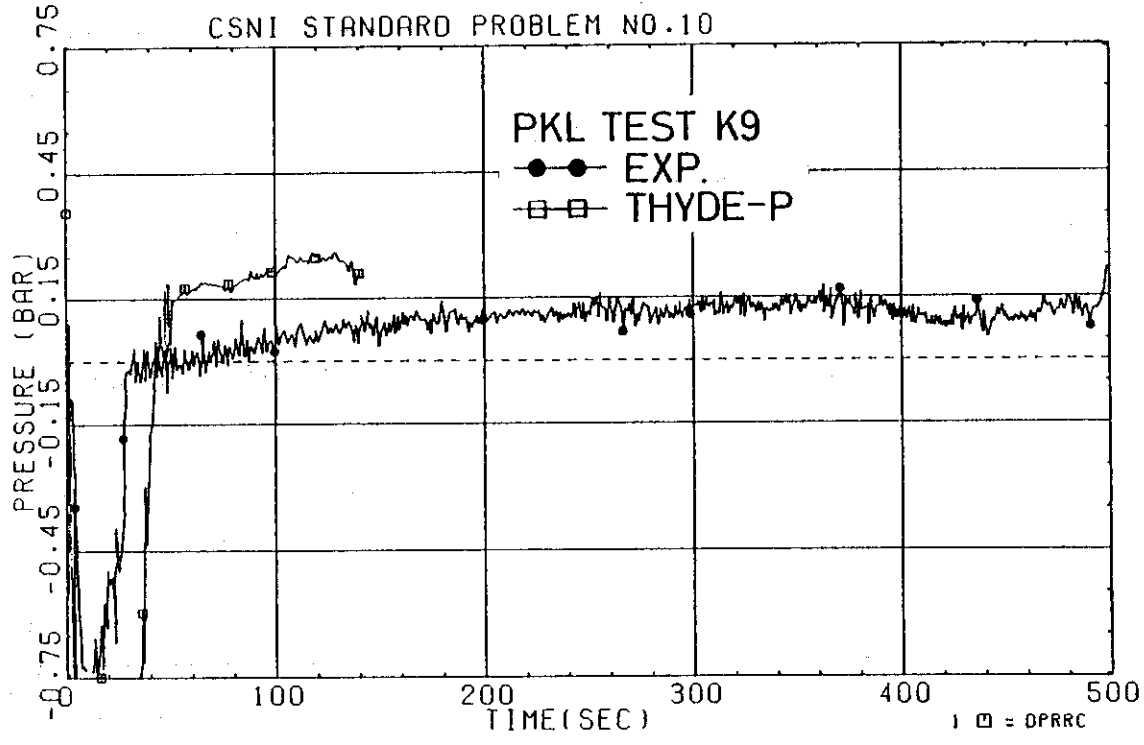

Fig. 5.16 Differential Pressure (Downcomer Nozzle-Break)

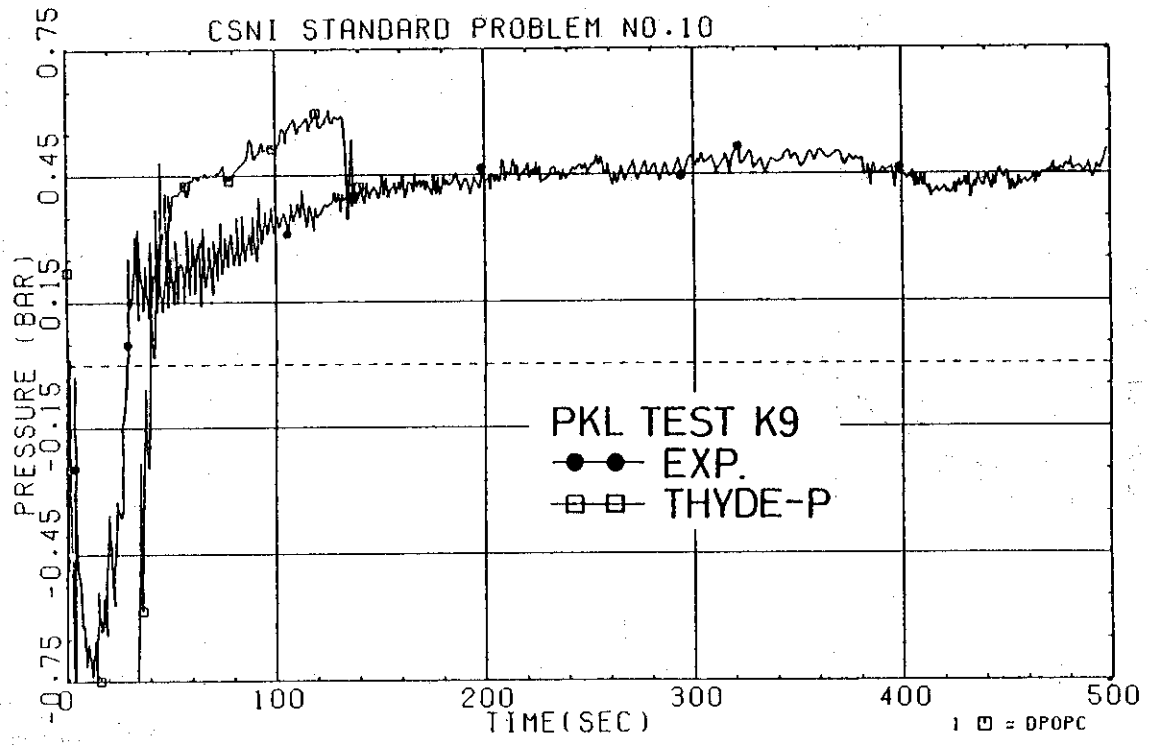

Fig. 5.17 Differential Pressure (Upper Plenum-Break)

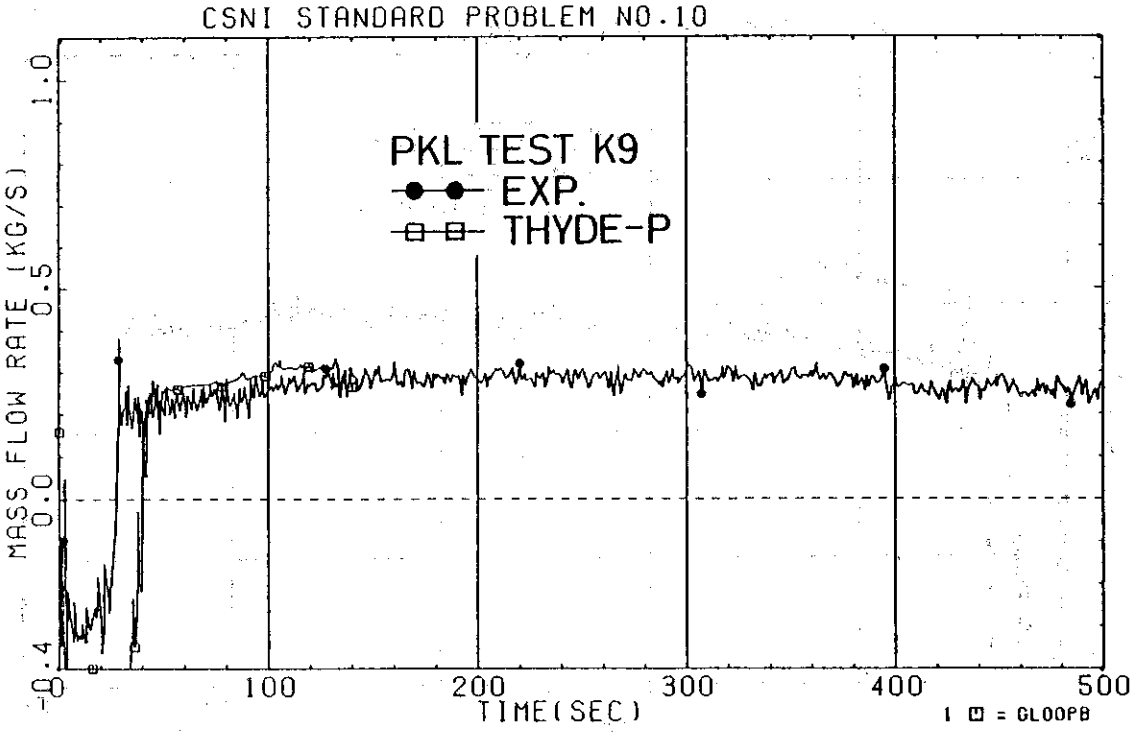

Fig. 5.18 Mass Flow Rate in Broken Loop

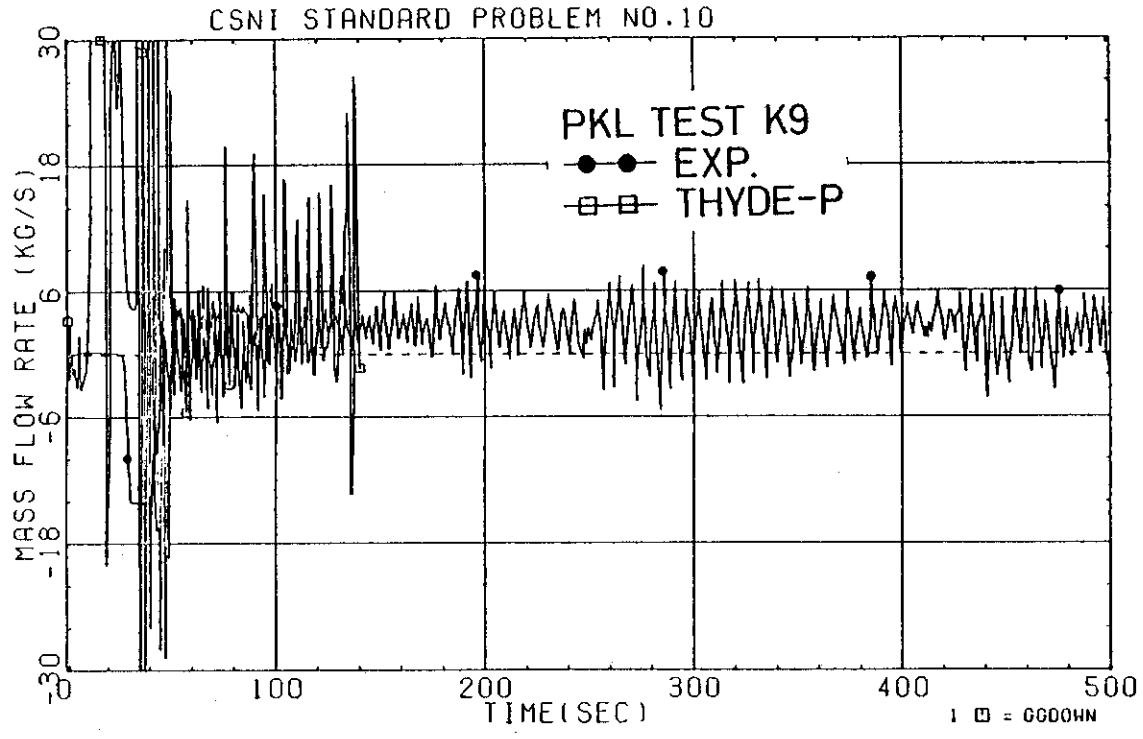

Fig. 5.19 Mass Flow Rate in Downcomer-Tube

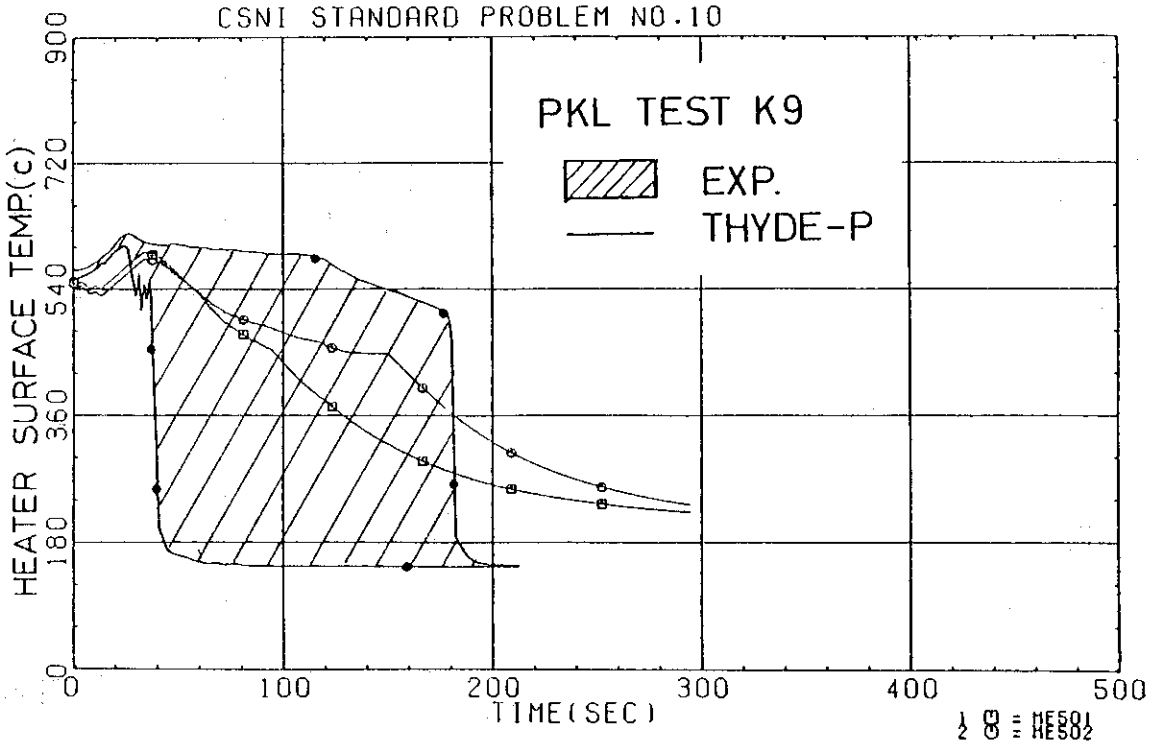

Fig. 5.20 Cladding Surface Temperatures at ME5
(without Phase Separation Model)

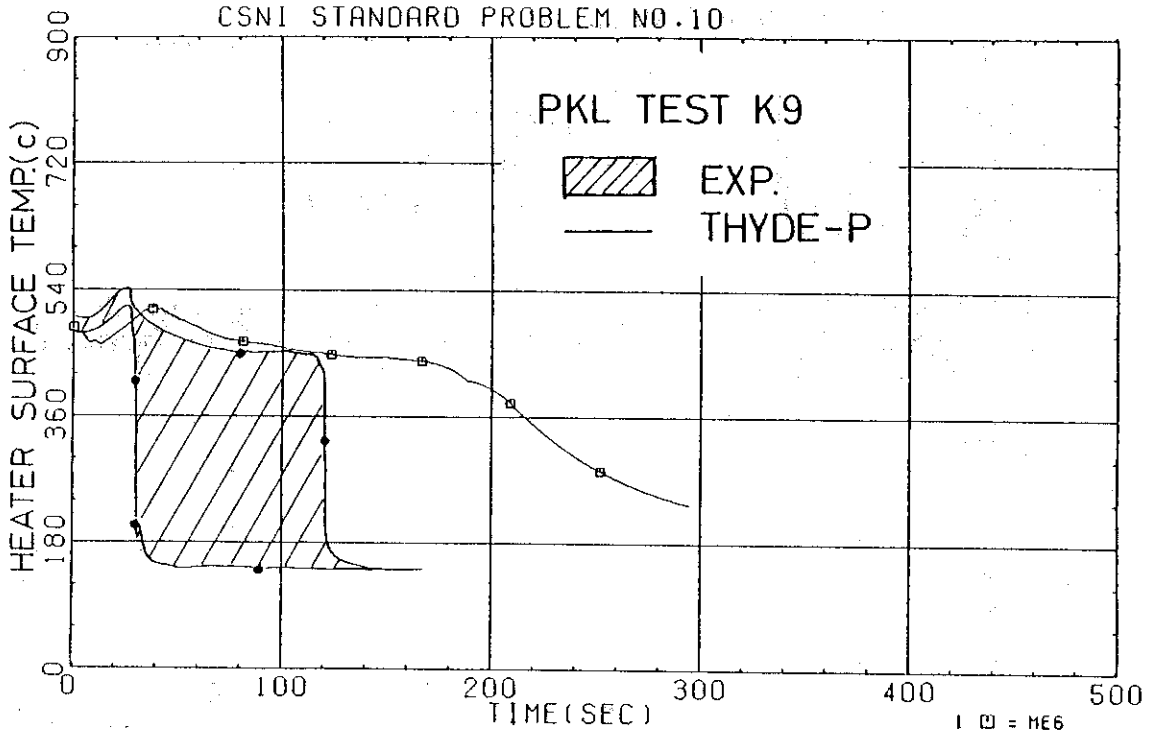

Fig. 5.21 Cladding Surface Temperatures at ME6
(without Phase Separation Model)

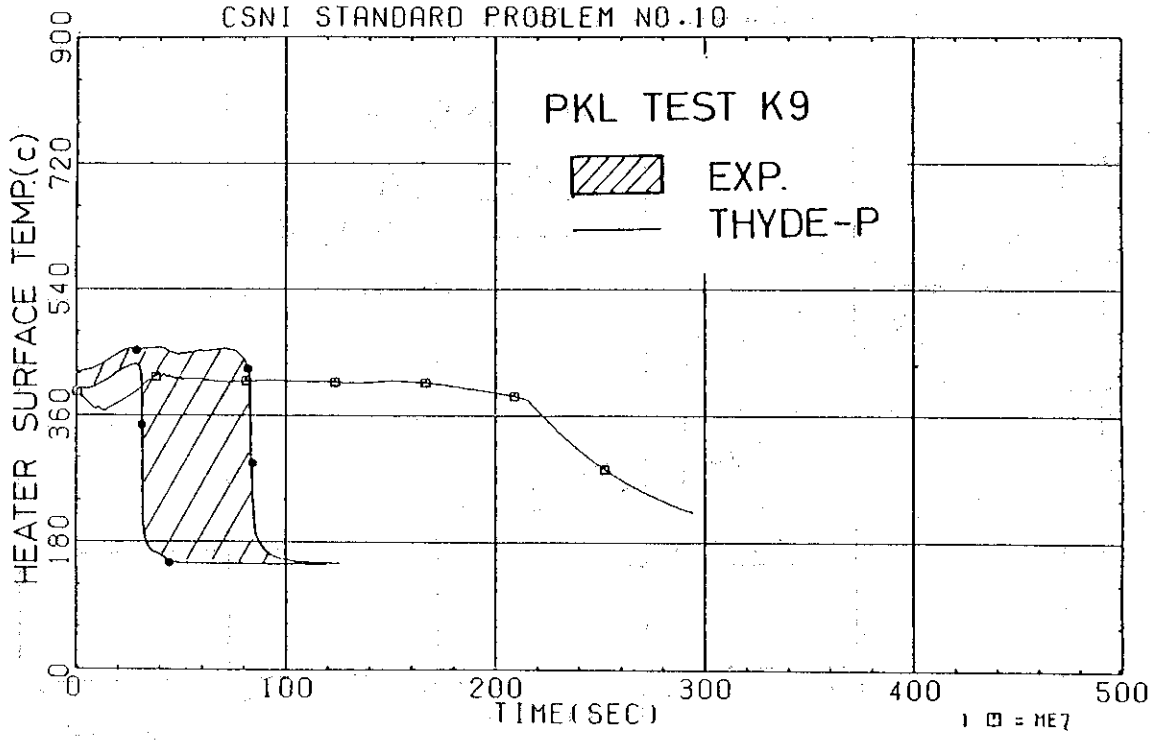

Fig. 5.22 Cladding Surface Temperatures at ME7
(without Phase Separation Model)

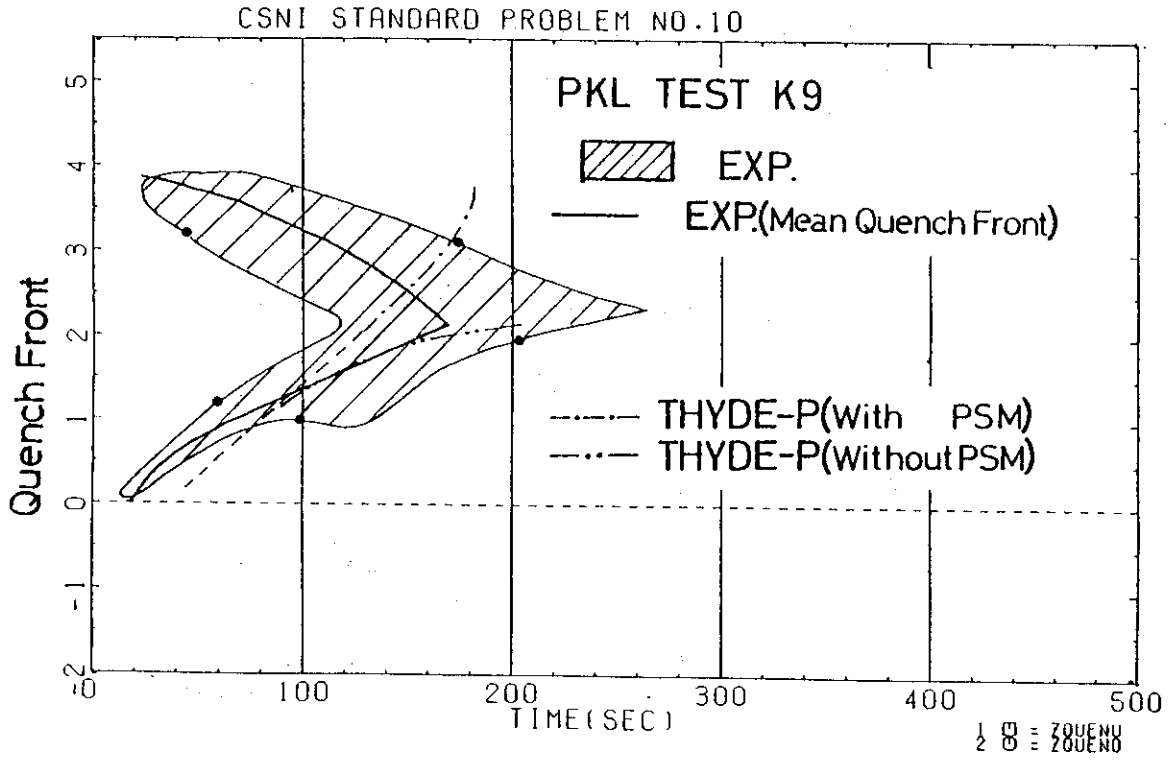

Fig. 5.23 Upper and Lower Quench Fronts
(without Phase Separation Model)

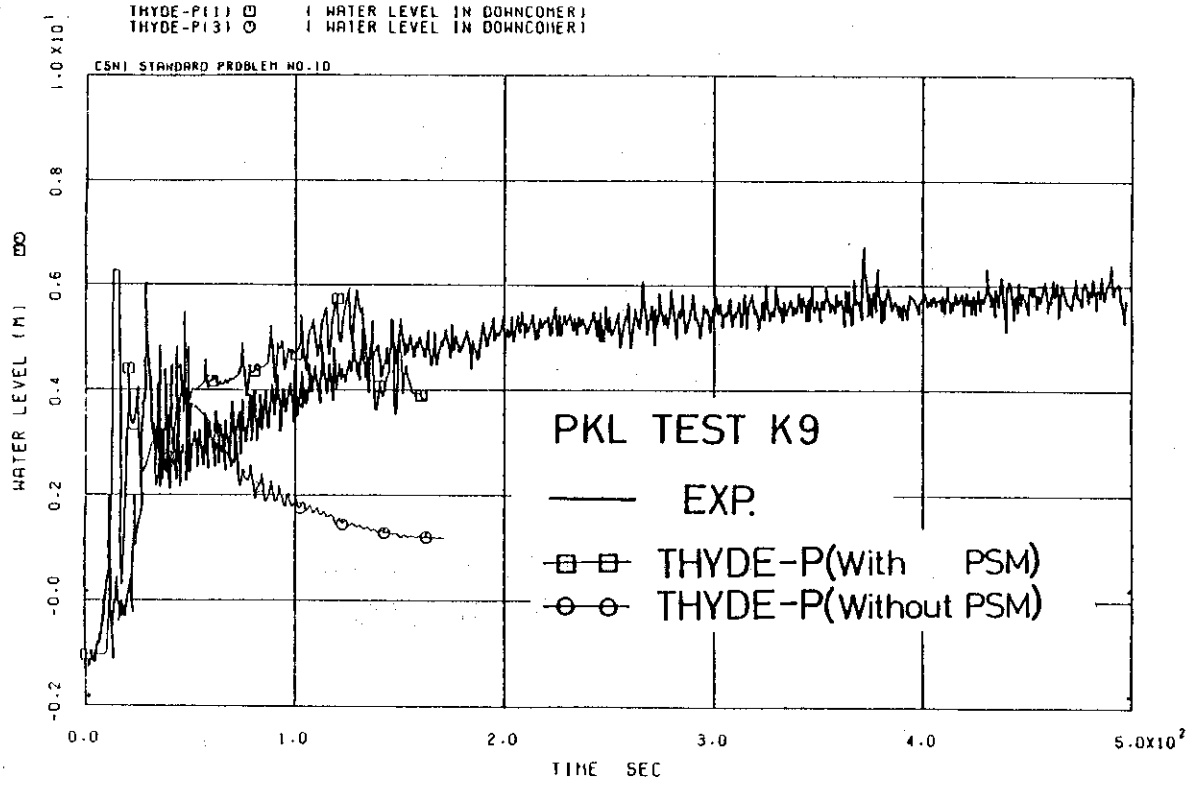

Fig. 5.24 Water Level in Downcomer

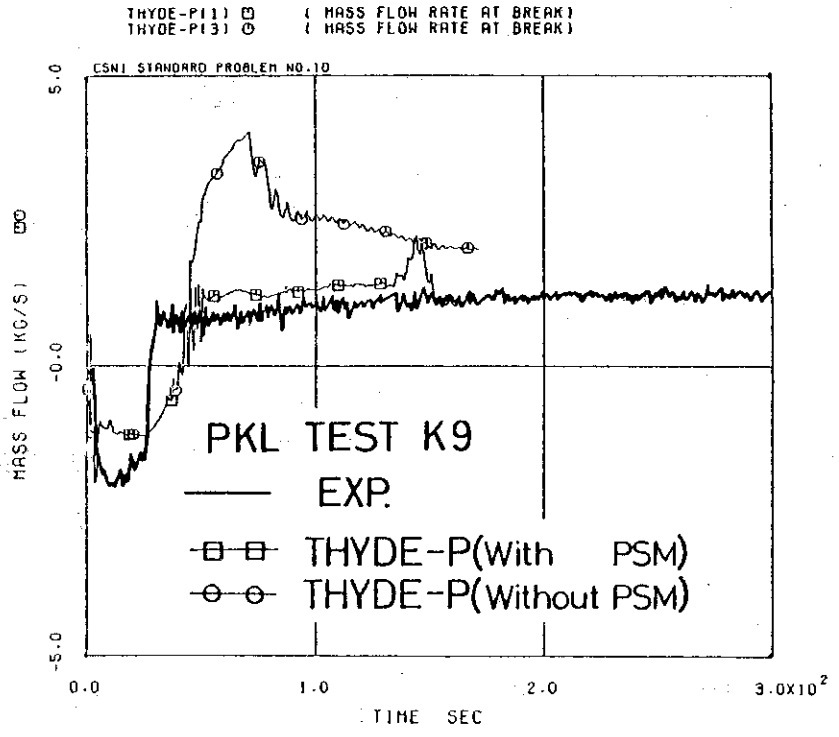

Fig. 5.25 Mass Flow Rate at Break

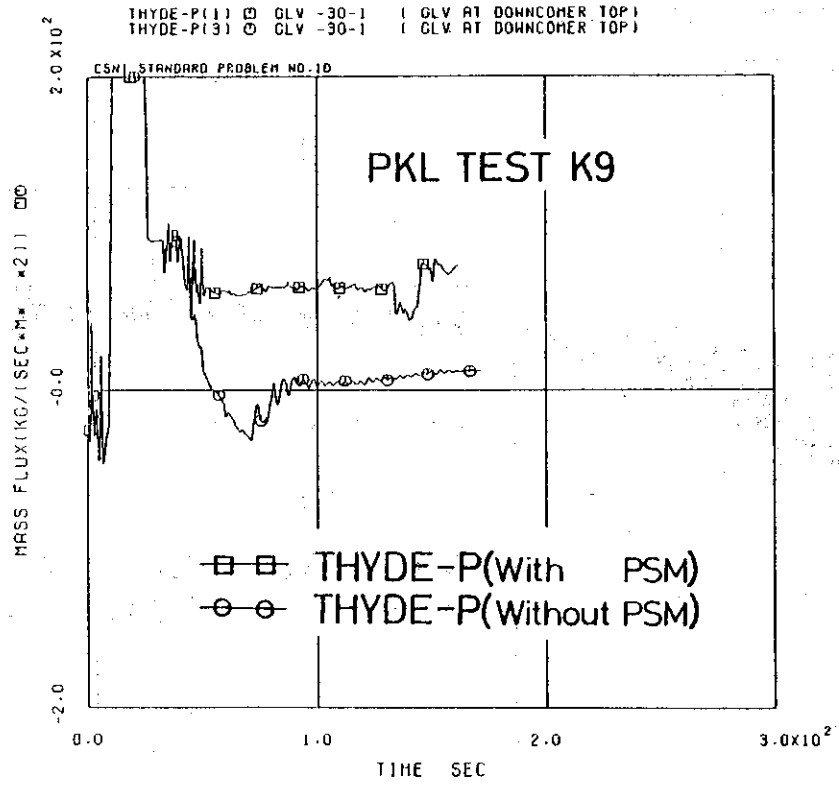

Fig. 5.26 Calculated Mass Fluxes at Downcomer Top

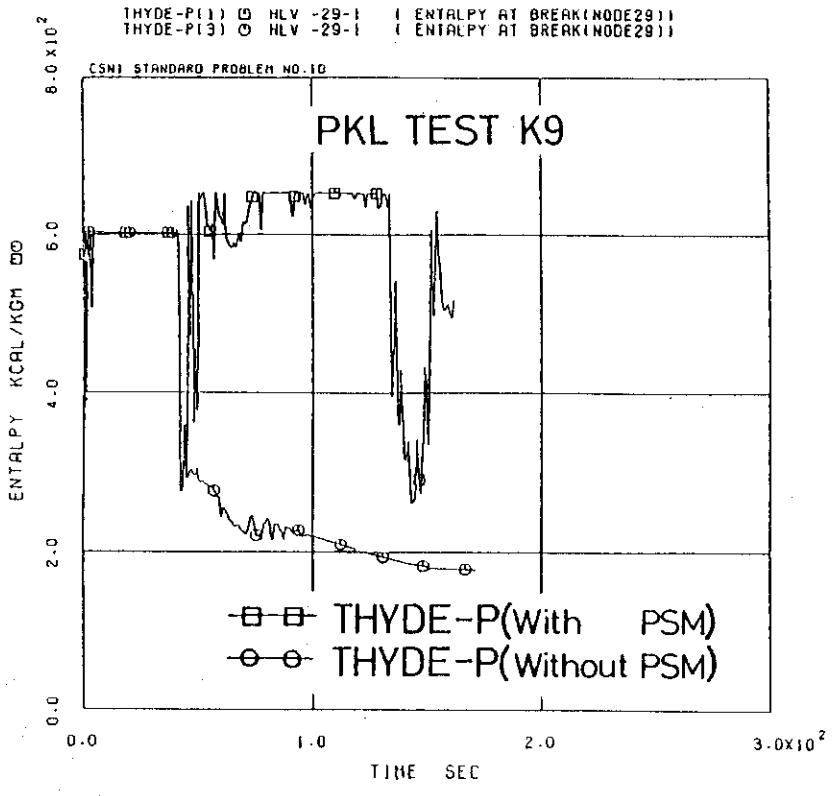

Fig. 5.27 Calculated Enthalpies at Node 29

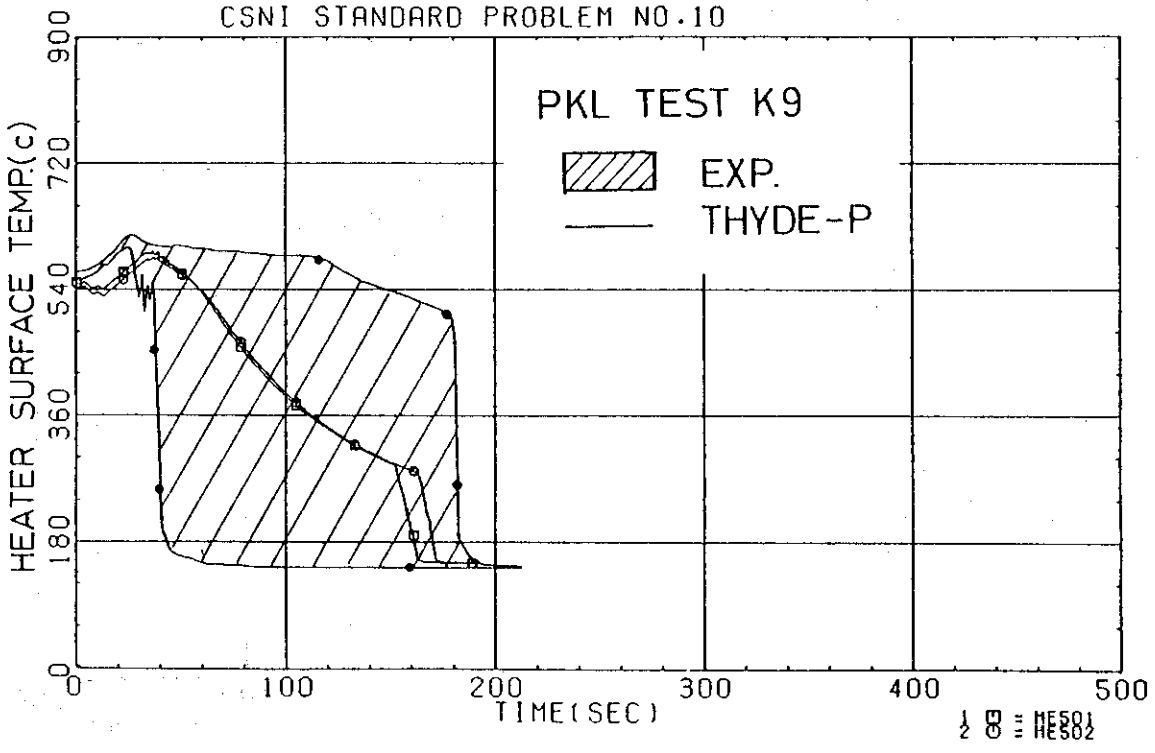

Fig. 5.28 Cladding Surface Temperatures at ME5
(without MSFBT Model)

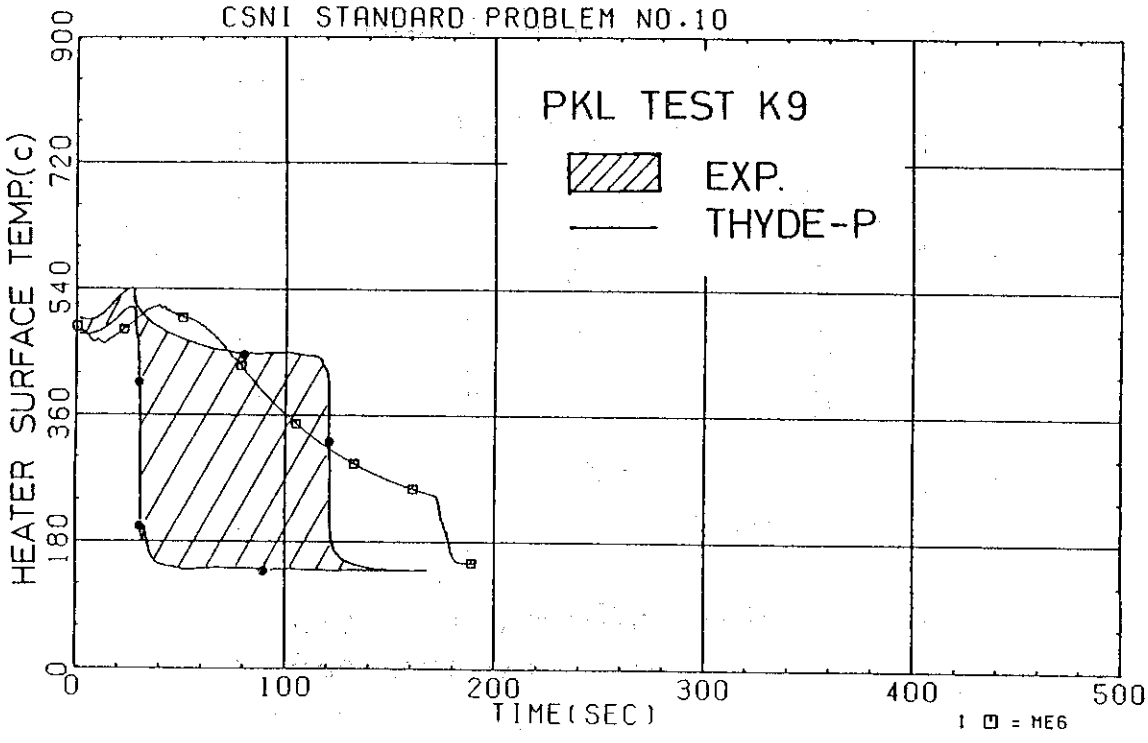

Fig. 5.29 Cladding Surface Temperatures at ME6
(without MSFBT Model)

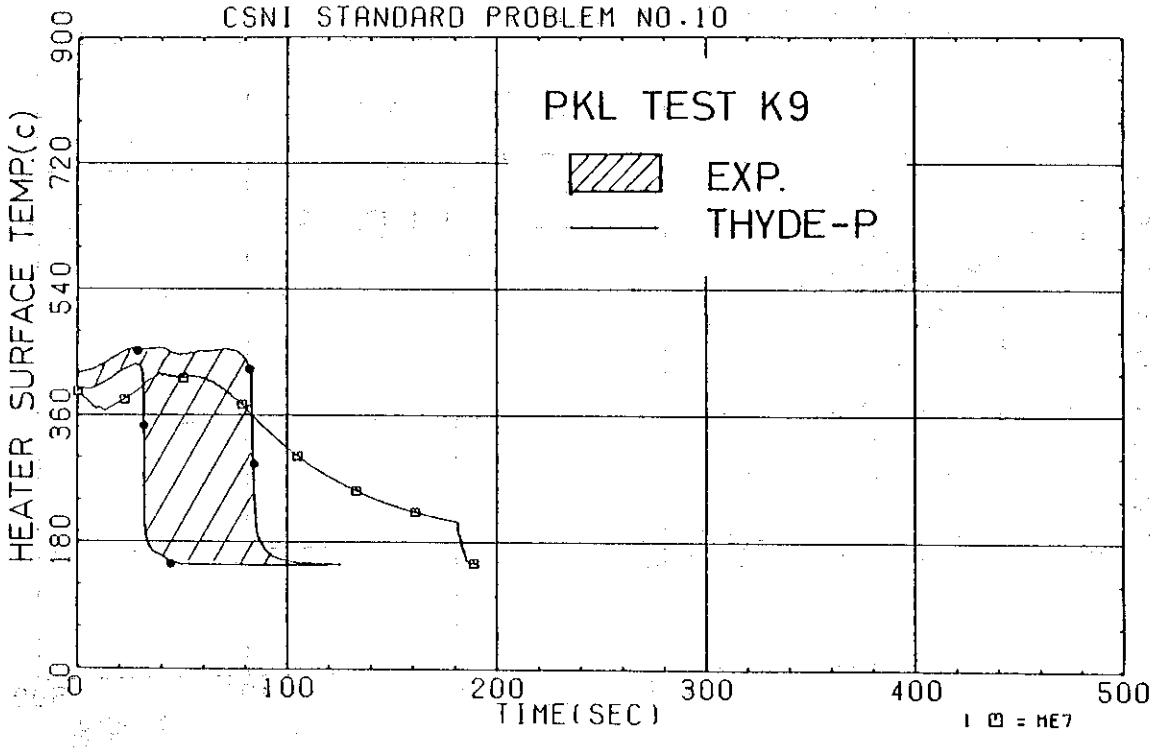

Fig. 5.30 Cladding Surface Temperatures at ME7
(without MSFBT Model)

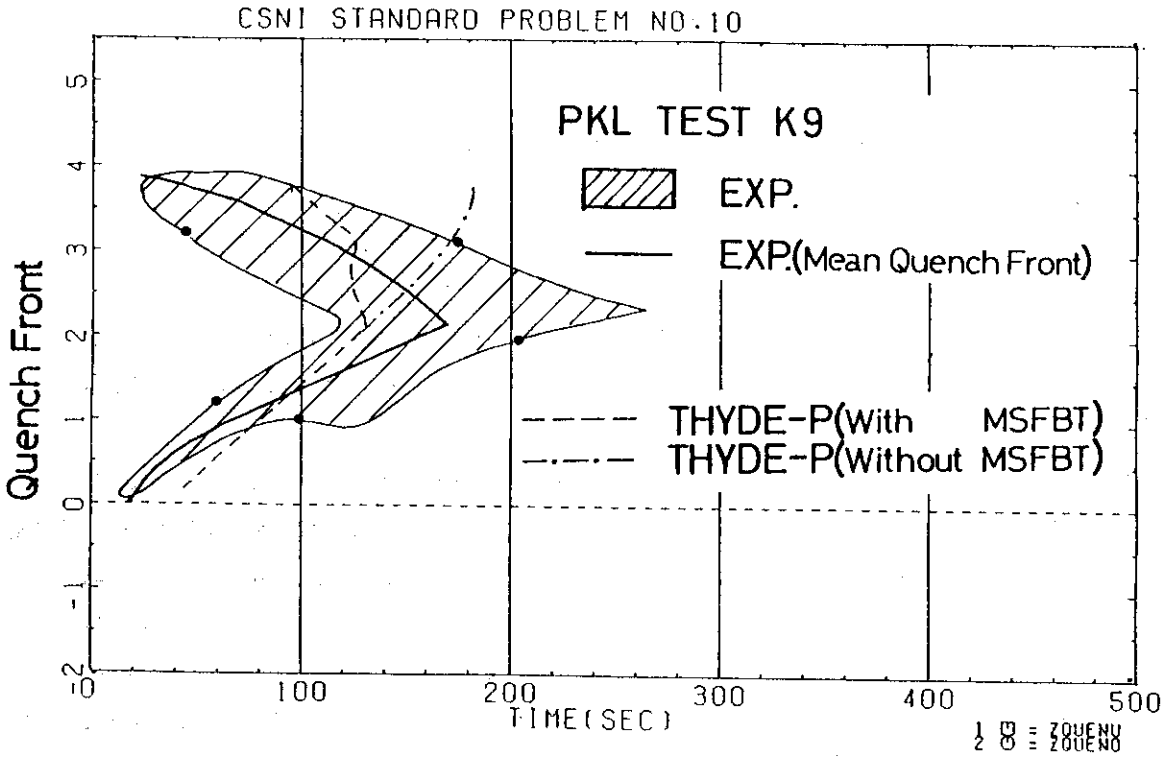

Fig. 5.31 Upper and Lower Quench Fronts

6. Conclusions

The major conclusions are as follows:

(1) The BE option of THYDE-P has predicted the overall trends of the experiment reasonably well.

(2) The maximum turn-around temperature is calculated at about 660°C, compared to the experimental value of 677°C.

(3) However, the time when the maximum temperature occures and the residence time above 590°C are considerably underestimated by the calculation with the THYDE-P code.

(4) In the present analysis, two types of quenching occur. One is caused by the mode change of the heat transfer from mode 4.3 (pool film boiling) to mode 4.4 (pool transition boiling) due to the ECC water flowing into the rod bundle through the lower plenum. The other is calculated when the cladding surface temperature decreases below the minimum film boiling temperature. The calculated results reproduce very well the experimental curve of the quench fronts.

(5) The flued dynamics and the system pressure history are satisfactorily predicted.

(6) The calculated break flow and water level in the downcomer after the reflood started are in good agreement with the experimental data only when complete phase separation is assumed to occur at the downcomer top.

Acknowledgments

The authors would like to express their sincere thanks to Mr. K. Sato, Chief of Reactor Safety Code Development Laboratory, for his valuable suggestions. The authors are also grateful to Messrs. M. Hirano, T. Shimizu, K. Muramatsu and M. Akimoto at the laboratory for their useful discussions and suggestions.

6. Conclusions

The major conclusions are as follows:

(1) The BE option of THYDE-P has predicted the overall trends of the experiment reasonably well.

(2) The maximum turn-around temperature is calculated at about 660°C, compared to the experimental value of 677°C.

(3) However, the time when the maximum temperature occures and the residence time above 590°C are considerably underestimated by the calculation with the THYDE-P code.

(4) In the present analysis, two types of quenching occur. One is caused by the mode change of the heat transfer from mode 4.3 (pool film boiling) to mode 4.4 (pool transition boiling) due to the ECC water flowing into the rod bundle through the lower plenum. The other is calculated when the cladding surface temperature decreases below the minimum film boiling temperature. The calculated results reproduce very well the experimental curve of the quench fronts.

(5) The flued dynamics and the system pressure history are satisfactorily predicted.

(6) The calculated break flow and water level in the downcomer after the reflood started are in good agreement with the experimental data only when complete phase separation is assumed to occur at the downcomer top.

Acknowledgments

The authors would like to express their sincere thanks to Mr. K. Sato, Chief of Reactor Safety Code Development Laboratory, for his valuable suggestions. The authors are also grateful to Messrs. M. Hirano, T. Shimizu, K. Muramatsu and M. Akimoto at the laboratory for their useful discussions and suggestions.

References

(1) Asahi, Y., "Description of THYDE-P Code (Preliminary Report of Methods and Models)", JAERI-M7751, 1978.

(2) Asahi, Y. and Hirano, M., "Verification Study of LOCA Analysis Code THYDE-P (Sample Calculation Run 10)", JAERI-M8560, 1979.

(3) Hirano, M. and Asahi, Y., "Through Analysis of LOFT L2-2 by THYDE-P Code (I) (Sample Calculation Run 30)", JAERI-M9535, 1981.

(4) Hirano, M., "Through Analysis of L2-3 by THYDE-P Code (Sample Calculation Run 40)", JAERI-M9765, 1981.

(5) Shimizu, T. and Asahi, Y., "Through Calculation of 1,100 MWe PWR Large Break LOCA by THYDE-P (Sample Calculation Run 20)", JAERI-M9819, 1981.

(6) Hirano, M., Shimuzu, T. and Asahi Y., "Analysis of LOFT Small Break Experiment L3-1 with THYDE-P code (CSNI International Standard Problem No.9 and THYDE-P Sample Calculation Run 50)", JAERI-M82-008, 1982.

(7) Brand, B., Kirmse, R. and Winkler, W., "Refill and Reflood Experiment in a Simulated PWR Primary System (PKL)", OECD-CSNI LOCA Standard Problem No.10, Specification, December 1979.

(8) Riedle, K., "Wiederauffüllversuche mit Berücksichtigung der Primärkreisläufe, Band 1: Beschreibung der Versuchsanlange", Förderungsverhaben BMFT 0036 B, KWU Reaktortechnik, RE 23/011/79, Erlangen, Oktober 1979.

(9) Brand, Mandl, Schmidt and Hein, "PKL Refill and Reflood Experiment Selected Results from Test K9", KWU Technical Report R51/22/79; Erlangen, 14. 12. 1979.

(10) Nguyen, D.L. and Winkler, W., "Comparison Report on OECD-CSNI LOCA Standard Problem No.10", CSNI Report No.64, September 1981.

(11) Dittus, F.W. and Boelter, L.M.K., "Heat Transfer in Automobile Radiations of The Tubular Tube", 2, No.13, PP.443-461, 1930.

(12) Jens, W.H. and Lottes, P.A., "Analysis of Heat Transfer, Burnout, Pressure Drop and Density Data for High-Pressure Water", ANL-4627, 1951.

(13) McEligot, D.M., Ormand, L.W. and Perkins, H.C., J. Trans. Amer. Soc. Mech. Engrs., 88, Series C, PP.239-245, May 1966.

(14) Groenevelt, D.C., "An Investigation of Heat Transfer in the Liquid Deficient Regime", Report AECC-3281, Chalk Rever, Ontario, December 1968.

(15) Pomeranz, M.L., "Film Boiling on a Horizontal Tube in Increased Gravity Fields", Journal of Heat Transfer, 86(1964) PP.213-219.

(16) T.R. Katsuma, et al., "RELAP4/MOD5 Users Manual Volume 1 (RELAP4/MOD5 Description)", ANCR-NUREG-1335 (Vol.1), 1976.

(17) Berenson, P.J.,"Film Boiling Heat Transfer from a Horizontal Surface", ASME paper no. 60-WA-147.

(18) Henry R.E., "A Correlation for the Minimum Film Boiling Temperature", AIChE Symposium Series, 138, Vol.70, 1974, PP.81-90.

(19) Bjornard, T.A. and Griffith, P., "PWR Blowdown Heat Transfer", Thermal and Hydraulic Aspects of Nuclear Reactor Safety, Vol.1 (American Society of Mechanical Enginneers, New York 1977), PP. 17-41.

Appendix A Input Data List

```
/                                                                                00000010
  PKL-REFLOOD EXPERIMENT(TEST K9) ANALYSIS BY THYDE-P CODE                       00000020
/     ***** DIMENSION DATA *****                                                 00000030
BB01                                                                             00000040
    0  0  9  3  8  51  47  2  1  2  0  2  6 14  5  5 1                          00000050
/                                                                                00000060
/     ***** MINOR EDIT DATA *****                                                00000070
BB02                                                                             00000080
PRE-28  GLE-28  GLA-29  GLE-30  GLE-11  GLE-25  TMP-11  TMP-25  TC1-09           00000090
/                                                                                00000100
/     ***** TIME STEP DATA *****                                                 00000110
BB03                                                                             00000120
SB0301                                                                           00000130
      0.2   0.2   100.0                                                        00000140
SB0302                                                                           00000150
      30   10  50   0  1.0E-3   1.0E-6      0.3    0.1                         00000160
SB0303                                                                           00000170
      30   10  50   0  4.0E-3   1.0E-6      1.0    0.1                         00000180
SB0304                                                                           00000190
      30   5   10   0 16.0E-3   1.0E-6   2000.0    0.1                         00000200
/                                                                                00000210
/     ***** TRIP CONTROL DATA *****                                              00000220
BB04                                                                             00000230
SB0410                                                                           00000240
      1   0    1   0  1000.0    0.0                                            00000250
SB0420                                                                           00000260
      5  49    1   0     0.4    0.0                                            00000270
SB0430                                                                           00000280
      5  50    1   0     0.4    0.0                                            00000290
SB0440                                                                           00000300
      4   1    1   0    80.0    0.0                                            00000310
SB0450                                                                           00000320
     -4   1    1   0  1010.0    0.0                                            00000330
SB0460                                                                           00000340
      3   0    1   0     0.0    0.0                                            00000350
SB0470                                                                           00000360
      2  27    1   0     0.1    0.0                                            00000370
SB0480                                                                           00000380
      2  13    1   0     0.1    0.0                                            00000390
/                                                                                00000400
BB05                                                                             00000410
      1     7000.0      360.0                                                  00000420
/                                                                                00000430
/     ***** LOOP NODE DATA *****                                                 00000440
BB06                                                                             00000450
SB0601                                                                           00000460
      1  1  44  1 0  160.000   0.139     0.0    3.035    0.371                  00000470
                      0.5      1.0       0.0    0.0                            00000480
SB0602                                                                           00000490
```

```
      2  1    1  2  0  159.9203  0.215     0.0     1.878     1.623          00000500
                        0.887    0.0572    0.      0.                       00000510
SB0603                                                                      00000520
      3  1    2  3  0  159.8145  0.315     0.0     0.256     0.256          00000530
                        2.48     1.83      3.38    9.52                     00000540
SB0604                                                                      00000550
      4  7    3  4  1  159.6327  0.019     0.0     0.965     0.965          00000560
                        0.0      0.0       0.0     0.0                      00000570
SB0605                                                                      00000580
      5  7    4  5  1  159.4117  0.019     0.0     0.965     0.965          00000590
                        0.0      0.0       0.0     0.0                      00000600
SB0606                                                                      00000610
      6  7    5  6  1  159.1907  0.019     0.0     6.725     6.510          00000620
                        0.0      0.0       0.0     0.0                      00000630
SB0607                                                                      00000640
      7  7    6  7  1  158.2449  0.019     0.0     4.725    -4.510          00000650
                        0.0      0.0       0.0     0.0                      00000660
SB0608                                                                      00000670
      8  7    7  8  1  158.2053  0.019     0.0     3.0      -3.0            00000680
                        0.0      0.0       0.0     0.0                      00000690
SB0609                                                                      00000700
      9  7    8  9  1  158.1376  0.019     0.0     0.930    -0.930          00000710
                        0.0      0.0       0.0     0.0                      00000720
SB0610                                                                      00000730
     10  1    9 10  0  158.0230  0.315     0.0     0.256    -0.256          00000740
                        9.52     3.38      1.83    2.48                     00000750
SB0611                                                                      00000760
     11  1   10 11  0  157.9631  0.215     0.0     1.836    -1.623          00000770
                        0.0      0.0       0.0572  0.887                    00000780
SB0612                                                                      00000790
     12  1   11 12  0  157.7450  0.139     0.0     5.322    -3.921          00000800
                        0.0      0.0       0.0     0.0                      00000810
SB0613                                                                      00000820
     13  8   12 13  0  157.1085  0.139     0.0     3.445     3.445          00000830
                        0.0      0.0       0.0     0.0                      00000840
SB0614                                                                      00000850
     14  1   13 45  0  164.5077  0.139     0.0     2.860     0.25           00000860
                        0.0      0.0       1.0     0.5                      00000870
SB0615                                                                      00000880
     15  1   44 14  0  160.000   0.0808    0.0     2.503     0.371          00000890
                        0.5      1.0       0.0     0.0                      00000900
SB0616                                                                      00000910
     16  1   14 15  0  159.9048  0.125     0.0     1.770     1.681          00000920
                        0.756    0.0573    0.0     0.0                      00000930
SB0617                                                                      00000940
     17  1   15 16  0  159.7929  0.195     0.0     0.198     0.198          00000950
                        3.59     2.37      4.44   12.3                      00000960
SB0618                                                                      00000970
     18  7   16 17  1  159.6116  0.019     0.0     0.965     0.965          00000980
                        0.0      0.0       0.      0.                       00000990
SB0619                                                                      00001000
     19  7   17 18  1  159.4178  0.019     0.0     0.965     0.965          00001010
                        0.       0.        0.      0.                       00001020
SB0620                                                                      00001030
```

```
     20  7  18 19 1  159.2240  0.019      0.0      6.725     6.510        00001040
                       0.       0.        0.       0.                     00001050
SB0621                                                                    00001060
     21  7  19 20 1  158.2782  0.019      0.0      4.725    -4.510        00001070
                       0.       0.        0.       0.                     00001080
SB0622                                                                    00001090
     22  7  20 21 1  158.1767  0.019      0.0      3.0      -3.0          00001100
                       0.       0.        0.       0.                     00001110
SB0623                                                                    00001120
     23  7  21 22 1  158.1090  0.019      0.0      0.930    -0.930        00001130
                       0.       0.        0.       0.                     00001140
SB0624                                                                    00001150
     24  1  22 23 0  158.0279  0.195      0.0      0.198    -0.198        00001160
                      12.3      4.44      2.37     3.59                   00001170
SB0625                                                                    00001180
     25  1  23 24 0  157.9631  0.125      0.0      1.738    -1.681        00001190
                       0.       0.        0.0573   0.756                  00001200
SB0626                                                                    00001210
     26  1  24 25 0  157.7547  0.0808     0.0      5.370    -3.898        00001220
                       0.       0.        0.       0.                     00001230
SB0627                                                                    00001240
     27  8  25 26 0  157.0536  0.0808     0.0      3.457     3.457        00001250
                       0.       0.        0.       0.                     00001260
SB0628                                                                    00001270
     28  1  26 27 0  164.2838  0.0808     0.0      1.243     0.215        00001280
                       0.       0.        0.0      1.0                    00001290
SB0629                                                                    00001300
     29  1  27 45 0  163.6850  0.0808     0.0      1.028     0.0          00001310
                       0.0      1.        1.       0.5                    00001320
SB0630                                                                    00001330
     30  4  45 28 0  163.4594  0.203      0.0      8.369    -7.334        00001340
                       0.3724   0.6850    1.0      0.5                    00001350
SB0631                                                                    00001360
     31  5  28 29 0  163.7843  0.42889    0.0      2.035     1.2115       00001370
                       0.       0.        0.       0.                     00001380
SB0632                                                                    00001390
     32  2  29 30 0  162.7152  0.24585    0.0      0.2317    0.165        00001400
                       8.68     8.90      0.       0.                     00001410
SB0633                                                                    00001420
     33  2  30 31 1  162.6006  0.24585    0.0      0.300     0.300        00001430
                       0.       0.        0.       0.                     00001440
SB0634                                                                    00001450
     34  2  31 32 1  162.4771  0.24585    0.0      0.400     0.400        00001460
                       0.       0.        0.       0.                     00001470
SB0635                                                                    00001480
     35  2  32 33 1  162.3470  0.24585    0.0      0.300     0.300        00001490
                       0.       0.        0.       0.                     00001500
SB0636                                                                    00001510
     36  2  33 34 1  162.2234  0.24585    0.0      0.300     0.300        00001520
                       0.       0.        0.       0.                     00001530
SB0637                                                                    00001540
     37  2  34 35 1  162.0897  0.24585    0.0      0.300     0.300        00001550
                       0.       0.        0.       0.                     00001560
SB0638                                                                    00001570
```

```
     38  2  35 36 1  161.9760  0.24585   0.0    0.300    0.300        00001580
                       0.        0.      0.      0.                  00001590
SB0639                                                               00001600
     39  2  36 37 1  161.8522  0.24585   0.0    0.300    0.300        00001610
                       0.        0.      0.      0.                  00001620
SB0640                                                               00001630
     40  2  37 38 1  161.7284  0.24585   0.0    0.400    0.400        00001640
                       0.        0.      0.      0.                  00001650
SB0641                                                               00001660
     41  2  38 39 1  161.5980  0.24585   0.0    0.300    0.300        00001670
                       0.        0.      0.      0.                  00001680
SB0642                                                               00001690
     42  2  39 40 1  161.4741  0.24585   0.0    0.300    0.300        00001700
                       0.        0.      0.      0.                  00001710
SB0643                                                               00001720
     43  2  40 41 1  161.3501  0.24585   0.0    0.400    0.400        00001730
                       0.        0.      0.      0.                  00001740
SB0644                                                               00001750
     44  2  41 42 1  161.2196  0.24585   0.0    0.300    0.300        00001760
                       0.        0.      0.      0.                  00001770
SB0645                                                               00001780
     45  2  42 43 0  161.0956  0.24585   0.0    0.2823   0.250        00001790
                       0.        0.      3.98   2.99                00001800
SB0646                                                               00001810
     46  6  43 44 0  160.6550  0.38987   0.0    1.6      1.6625       00001820
                       0.        0.      0.      0.                  00001830
SB0647                                                               00001840
     47 13  45 46 0    1.0      0.139     0.0    2.0     -1.0         00001850
                       0.        0.      0.      0.                  00001860
SB0648                                                               00001870
     48 13  44 47 0    2.5      0.30589   0.0   10.432   -6.763       00001880
                       1.5       1.5      0.      0.                  00001890
/                                                                    00001900
/    ***** JUNCTION DATA *****                                       00001910
BB07                                                                 00001920
       1   1   0.0                                                   00001930
       2   1   0.0                                                   00001940
       3   1   0.0                                                   00001950
       4   1   0.0                                                   00001960
       5   1   0.0                                                   00001970
       6   1   0.0                                                   00001980
       7   1   0.0                                                   00001990
       8   1   0.0                                                   00002000
       9   1   0.0                                                   00002010
      10   1   0.0                                                   00002020
      11   1   0.0                                                   00002030
      12   1   0.0                                                   00002040
      13   1   0.0                                                   00002050
      14   1   0.0                                                   00002060
      15   1   0.0                                                   00002070
      16   1   0.0                                                   00002080
      17   1   0.0                                                   00002090
      18   1   0.0                                                   00002100
      19   1   0.0                                                   00002110
```

```
       20    1    0.0                                                          00002120
       21    1    0.0                                                          00002130
       22    1    0.0                                                          00002140
       23    1    0.0                                                          00002150
       24    1    0.0                                                          00002160
       25    1    0.0                                                          00002170
       26    1    0.0                                                          00002180
       27    1    0.0                                                          00002190
       28    1    0.0                                                          00002200
       29    1    0.0                                                          00002210
       30    1    0.0                                                          00002220
       31    1    0.0                                                          00002230
       32    1    0.0                                                          00002240
       33    1    0.0                                                          00002250
       34    1    0.0                                                          00002260
       35    1    0.0                                                          00002270
       36    1    0.0                                                          00002280
       37    1    0.0                                                          00002290
       38    1    0.0                                                          00002300
       39    1    0.0                                                          00002310
       40    1    0.0                                                          00002320
       41    1    0.0                                                          00002330
       42    1    0.0                                                          00002340
       43    1    0.0                                                          00002350
       44    2    0.2112                                                       00002360
       45    3    0.0166                                                       00002370
       46    7    0.0                                                          00002380
       47    8    0.0                                                          00002390
/                                                                             00002400
/    ***** MIXING JUNCTION DATA *****                                         00002410
BB08                                                                          00002420
SB0801                                                                        00002430
      44  3  1  15  48  0  0.75   0.25   0.0   0.0                            00002440
SB0802                                                                        00002450
      45  2 30  47  0   0  1.0    0.0    0.0   0.0                            00002460
/                                                                             00002470
/    ***** PUMP INJECTION DATA *****                                          00002480
BB09                                                                          00002490
SB0901                                                                        00002500
       1   46    50.488                                                       00002510
       8                                                                      00002520
      0.0   10.12    1.5   10.26    5.0   9.34    10.2   8.05                 00002530
     17.6    6.81   24.9    5.98   26.0   1.90  2000.0   1.9                  00002540
/                                                                             00002550
/    ***** PUMP DATA *****                                                    00002560
BB10                                                                          00002570
SB1001                                                                        00002580
  27  1 1185.0  5.58  4.33E4  105.0 749.0  1150.0  3460.0 -0.5  0.0          00002590
SB1002                                                                        00002600
  13  1 1185.0 16.74  4.33E4  105.0 749.0  1150.0  3460.0 -0.5  0.0          00002610
/                                                                             00002620
/   ***** PUMP DATA TABLE *****                                              00002630
BB11                                                                          00002640
SB1101                                                                        00002650
```

```
  1
  14
 -1.0   1.56  0.18 -0.85  1.33   0.34  -0.8  1.28  0.40  -0.72
  1.30  0.48 -0.62  1.35  0.556 -0.5    1.36 0.67 -0.34   1.34
  0.77 -0.21  1.29  0.84 -0.11   1.23   0.89 0.0   1.22   0.95
  0.25  1.16  1.16  0.5   1.13   1.35   0.75 1.07  1.62   1.0   0.98 1.94
  11
 -1.0   0.18 1.56 -0.75 -0.13 1.12 -0.50 -0.32 0.9  -0.32 -0.4   0.82
 -0.16 -0.42 0.76  0.0  -0.39 0.71  0.16 -0.28 0.71  0.32  0.16  0.76
  0.5   0.01 0.90  0.75  0.4  1.33  1.0   0.98 1.94
  14
 -1.0  0.7  -1.42 -0.9  0.7  -1.32 -0.8  0.68 -1.23 -0.7 0.63 -1.14
 -0.6  0.53 -1.07 -0.50 0.47 -0.99 -0.4  0.46 -0.91 -0.3 0.45 -0.84
 -0.2  0.45 -0.77  0.0  0.48 -0.64  0.25 0.55 -0.49  0.5 0.66 -0.34
  0.75 0.83 -0.2   1.0  1.02 -1.10
  13
  -1.0 -1.42 0.7  -0.8 -1.12 0.5 -0.6 -0.82 0.4 -0.5 -0.68  0.39
  -0.4 -0.55 0.38 -0.2 -0.28 0.33 0.0 -0.08 0.28 0.11 0.0   0.25
   0.25 0.12 0.22  0.50 0.33 0.14 0.75 0.61 0.03 0.92 0.82  0.01
   1.0 1.02 -0.10
   2
   0.0  1.0  1000.0   0.5
 2
  -1.0  -50.0  1.0   50.0
 6  6
  0.0  0.2  0.4  0.6  0.8  1.0
  0.0  0.0  0.0  0.0  0.0  0.0  0.0
  0.2  0.0  3.065E-5  7.7239E-5  1.3263E-4  1.946E-4  2.6207E-4
  0.4  0.0  4.866E-5  1.2261E-4  2.1053E-4  3.0996E-4 4.1602E-4
  0.6  0.0  6.376E-5  1.6066E-4  2.7587E-4  4.0485E-4 5.4514E-4
  0.8  0.0  7.7239E-5 1.9463E-4  3.3419E-4  4.9044E-4 6.6037E-4
  1.0  0.0  8.9628E-5 2.2585E-4  3.878E-4   5.691E-4  7.6631E-4
/
/     ***** BREAK POINT DATA *****
BB13
    27    0.0    0.4    0.8    0.6   0.6   0.8    0.6    0.6
    18
    0.0 1.0       7.5 2.7       15.0 4.69     40.0 4.69     80.0 4.69
   90.0 4.45    100.0 4.26    110.0 4.01    120.0 3.85    130.0 3.78
  155.0 3.71    180.0 3.71    205.0 3.67    230.0 3.57    280.0 3.46
  380.0 3.20    430.0 3.06   1000.0 3.06
/
/    ***** STEAM GENERATOR DATA *****
BB15
SB1501
   49  90   4   9   6   1   0.1591    8.5858    1.0     0.5    0.034167    0.0095
   12.94     4.2       273.7    9.6    0.99   0.2077     56.59
   -2.       -2.        -1.8   -1.8   -1.9   -1.9
    3.0E-5 80.0         0.5    0.5    0.5
   3
    0.0    1.0      1.0     1.0     1.0     1.0   1.0   1.0   1000.0   1.0    1.0   0.0
SB1502
    50   30    18   23     6    1   0.0624   8.57628   1.0   0.5   0.03638    0.0095
     5.38     4.2       273.7     3.8      0.99     0.2459      54.04
```

```
    -2.     -2.       -1.8  -1.8   -1.9   -1.9                              00003200
       1.0E-5 80.0   0.5   0.5  0.5                                         00003210
     3                                                                      00003220
      0.0  1.0   1.0   1.0  1.0 1.0 1.0 1.0  1000.0 1.0 1.0 0.0            00003230
/                                                                           00003240
/  **** CORE DATA ****                                                      00003250
BB16                                                                        00003260
  337   32   45    1                                                       00003270
  5.375E-3  1.43E-2     0.0                                               00003280
  0.0   3.94   5.30   6.41   6.41   7.22   7.22   7.22   7.22   6.41      00003290
  6.41  5.30   3.94   0.0                                                 00003300
  1   1   2   1   2                                                       00003310
  0.  0.  1.0 0.  0.                                                      00003320
/                                                                           00003330
/  **** HEATER PHYSICAL PROPERTIES ******                                  00003340
BB17                                                                        00003350
/  -- HEATER POWER DATA --                                                 00003360
  2                                                                         00003370
  0.0   2.0   2000.0   2.0                                                 00003380
/  -- DENSITY DATA -- NO.1                                                 00003390
  2                                                                         00003400
  10.0  3150.0  2000.0  3150.0                                            00003410
/  -- DENSITY DATA -- NO.2                                                 00003420
 2                                                                          00003430
  10.0  8300.0  2000.0  8300.0                                            00003440
/  -- CP DATA  --     NO.1                                                 00003450
 5                                                                          00003460
 100. 0.248  300. 0.278  500. 0.292  1000. 0.310  1300. 0.319              00003470
/  -- CP DATA  --     NO.2                                                 00003480
 2                                                                          00003490
 100. 0.12  1300. 0.12                                                    00003500
/  -- CONDUCTIVITY DATA --    NO.1                                         00003510
 12  2                                                                     00003520
 100.  200.  300.  400.  500.  600.  700.  800.  900.  1000.               00003530
1100.  1200.                                                              00003540
2000.  4000. 2000. 4000. 2000. 4000. 2000.  4000.                         00003550
2000.  4000. 2000. 4000. 2000. 4000. 2000.  4000.                         00003560
2000.  4000. 2000. 4000. 2000. 4000. 2000.  4000.                         00003570
 4.78E-3  4.78E-3  4.02E-3  4.02E-3  3.25E-3  3.25E-3                       00003580
 2.51E-3  2.51E-3  1.94E-3  1.94E-3  1.58E-3  1.58E-3                       00003590
 1.36E-3  1.36E-3  1.20E-3  1.20E-3  1.10E-3  1.10E-3                       00003600
 1.05E-3  1.05E-3  1.03E-3  1.03E-3  1.03E-3  1.03E-3                       00003610
/  -- CONDUCTIVITY DATA --    NO.1                                         00003620
5  2                                                                      00003630
 20.  250.  550.  800.  1300.                                             00003640
 1000.  10000.  1000.  10000.  1000.  10000.                              00003650
 1000.  10000.  1000.  10000.                                             00003660
 2.89E-3  2.89E-3  3.90E-3  3.90E-3  5.11E-3  5.11E-3                      00003670
 6.12E-3  6.12E-3  8.08E-3  8.08E-3                                        00003680
/                                                                           00003690
/  **** OTHER DATA ****                                                    00003700
BB22                                                                        00003710
   0. 1.4  1.4  0.                                                        00003720
BEND                                                                        00003730
6                                                                           00003740
   0  0    0   0   55000   80.                                            00003750
   0. 17.  0.  0.  17.     17.5                                           00003760
0                                                                           00003770
20  0.04                                                                  00003780
13   14    29    30   31   45   47   32   33   34                        00003790
0.5  0.5   0.1   1.   0.5  0.3  1.   0.3  0.3  0.3                       00003800
35   36    37    38   39   40   41   42   43   44                        00003810
0.3  0.3   0.3   0.3  0.3  0.3  0.3  0.3  0.3  0.3                       00003820
```

Appendix B Nomenclature

Alphabetic Symbols

A	Flow area
C_p	Specific heat capacity
g	Gravitational acceleration
G	Mass flux
G_{min}	Minimum mass flux for forced convection condition
h	Enthalpy
h_{fg}	Latent heat
h_{out}	Outlet enthalpy
I	Drift energy flux
ℓ	Drift energy flow
k	Loss Coefficient
$\tilde{k}$	Thermal conductivity
L	Node length
p	Pressure
T	Temperature
T_{HN}	Homogeneous nucleation temperature
T_{MSFB}	Minimum stable film boiling temperature
u_{gj}	Drift velocity
u_r	Relative velocity
x	Equilibrium quality
x_c	Threshold quality defined in eq. (3.1.2)
$\tilde{x}_c$	Threshold quality used in eq. (3.4.3)

Greek Symbols

α	Equilibrium void fraction
α_c	Threshold void fraction used in eq. (3.3.3)
ρ	Equilibrium density
ϕ	Heat flux
ϕ_c	Heat flux defined in eq. (3.1.2)
σ	Surface tension
Λ	Enthalpy flux

Subscripts

CHF	Critical heat flux
fs	Saturated flux
gs	Saturated steam
j	Junction number
l	Liquid phase
n	Node number
sat	Saturated property

Superscripts

A	Inlet point of node
E	Outlet point of node
f	Forward flow
j	Junction number
n	Node number
r	Reverse flow